Accepted Manuscript

Extracellular vesicles enhance the targeted delivery of immunogenic oncolytic adenovirus and paclitaxel in immunocompetent mice

M. Garofalo, A. Villa, N. Rizzi, L. Kuryk, B. Rinner, V. Cerullo, M. Yliperttula, V. Mazzaferro, P. Ciana

PII: S0168-3659(18)30725-9
DOI: https://doi.org/10.1016/j.jconrel.2018.12.022
Reference: COREL 9572

To appear in: *Journal of Controlled Release*

Received date: 2 August 2018
Revised date: 30 November 2018
Accepted date: 12 December 2018

Please cite this article as: M. Garofalo, A. Villa, N. Rizzi, L. Kuryk, B. Rinner, V. Cerullo, M. Yliperttula, V. Mazzaferro, P. Ciana , Extracellular vesicles enhance the targeted delivery of immunogenic oncolytic adenovirus and paclitaxel in immunocompetent mice. Corel (2018), https://doi.org/10.1016/j.jconrel.2018.12.022

This is a PDF file of an unedited manuscript that has been accepted for publication. As a service to our customers we are providing this early version of the manuscript. The manuscript will undergo copyediting, typesetting, and review of the resulting proof before it is published in its final form. Please note that during the production process errors may be discovered which could affect the content, and all legal disclaimers that apply to the journal pertain.

ACCEPTED MANUSCRIPT

Extracellular vesicles enhance the targeted delivery of immunogenic oncolytic adenovirus and paclitaxel in immunocompetent mice

M. Garofalo[1,2], A. Villa[1], N. Rizzi[3], L. Kuryk [4,5],B. Rinner[6], V. Cerullo[7], M. Yliperttula[2], V. Mazzaferro[1,8], P. Ciana[1*]*

Affiliations

[1]Department of Oncology and Hemato-Oncology, Center of Excellence on Neurodegenerative Diseases, University of Milan, Milan, Italy

[2]Division of Pharmaceutical Biosciences and Drug Research Program, University of Helsinki, Helsinki, Finland

[3] Center of Excellence on Neurodegenerative Diseases, University of Milan, Milan, Italy

[4]Targovax Oy, Clinical Science, Helsinki, Finland

[5]National Institute of Public Health – National Institute of Hygiene, Department of Virology, Warsaw, Poland

[6] Biomedical Research, Core Facility Alternative Biomodels and Preclinical Imaging, Medical University of Graz, Austria

[7] University of Helsinki, Drug Research Program, ImmunoVirothearpy Lab, Faculty of Pharmacy, Helsinki, Finland

[8] Istituto Nazionale Tumori Fondazione IRCCS, National Cancer Institute, Milan, Italy

[*]*co-correspondance*

Corresponding authors:

E-mail address: paolo.ciana@unimi.it (P.Ciana)

mariangela.garofalo@unimi.it (M.Garofalo)

ACCEPTED MANUSCRIPT

ACCEPTED MANUSCRIPT

ABSTRACT

Extracellular vesicles (EVs), are naturally occurring cargo delivery tools with the potential to be used as drug vehicles of single agents or combination therapies. We previously demonstrated that human lung cancer cell-derived EVs could be used for the systemic delivery of oncolytic virus (OVs) and chemotherapy drugs such as paclitaxel (PTX), leading to enhanced anti-tumor effects in nude mice. In the current work, we evaluated the biodistribution of EVs by using bioluminescence and fluorescence imaging technologies, thus proving the ability of these EVs-formulations to specifically target the neoplasia, while leaving other body tissues unaffected. Moreover, *in vivo* imaging of NFκB activation in an immunocompetent reporter mouse model allowed to demonstrate the selective ability of EVs to induce tumor-associated inflammatory reactions, which are characterized by immunogenic cell death and CD3+/CD4+/CD8+ T-cell infiltration. While EVs have the potential to induce a systemic immune reaction by pro-inflammatory cytokines, our study provides compelling evidences of a localized inflammatory effect in the peritumoral area. Collectively, our findings strongly support the systemic administration of EVs formulations with OVs alone or in combination with chemotherapy agents as a novel strategy aimed at treating primary and metastatic cancers.

Key words: extracellular vesicles, oncolytic adenoviruses, drug delivery, lung cancer, immunocompetent cancer mouse models, *in vivo* imaging.

ACCEPTED MANUSCRIPT

INTRODUCTION

ACCEPTED MANUSCRIPT

Tumors are heterogeneous complexes of cells [1] able to grow in an uncontrolled way and to develop mechanisms for evading immune responses [2–4]. Indeed, the tumor itself can enhance the suppression of antitumor immunity [5] by expressing inhibitory ligands such as: programmed death-ligands (PD-1, PD-L1, PD-L2), NKG2D, MICA/B), [6] suppressors of NK and T-cell activation [7] and accelerate the production of immunosuppressive CD4+ T cells [8]. Therapies aimed at activating the host immune response [9] have been proven useful as monotherapy or in combination with other anti-neoplastic agents [10–14], particularly when tumors acquire resistance to standard therapies and become metastatic [15,16]. Among the novel therapeutic strategies aiming at targeting the host immune response against the tumor, treatment with OVs is one of the most promising approach [17–20] since it combines the cytolytic activity with the ability of the virus to activate the immune system [21,22]. OVs can exhibit natural tumor-selective tropism or be genetically modified for cancer cell-restricted replication (adenovirus, poliovirus, herpes simplex) [23]. Moreover, OVs are purposefully engineered to preferentially infect, replicate in and kill cancer cells instead of normal cells [24–29]. Clinical trials testing OVs treatments as monotherapy have provided encouraging results in terms of safety [30,31]: in most of these trials, the route of administration of choice was intratumoral (i.t.) and achieved proof-of-principles results with the demonstration of tumor lysis, immunogenic cell death and production of type-I IFN [32]. However, the efficacy has remained limited [33]. Since not all tumours can be treated i.t. and since OVs monotherapy may not be sufficient to eradicate cancer cells, novel strategies addressing the issue of efficacy and safety for the systemic delivery of OVs alone or in combination with other anti-cancer agents are in high demand.

Extracellular vesicles (EVs), are nano- to micron-sized lipid membrane-bound vesicles secreted into the extracellular environment transporting proteins, lipids and nucleic acids from cell to cell [34,35]. They are naturally occurring cargo delivery agents with the potential to be used as vehicles for drug delivery [36–38], in particular for the combined administration of OVs with chemotherapy agents [39]; in addition to endogenous uptake mechanisms, their lipid membrane may further improve the permeability of drugs into target cells [40,41]. It has been reported that EVs have intrinsic cell targeting properties: cell surface structures, such as tetraspanins and integrins, may direct the EV uptake towards specific cells and protect therapeutic agents from opsonization and recognition by phagocytes, leading to a longer half-life and reduced side-effects in healthy cells and tissues [42,43]. EVs have been shown to be safe in several clinical trials [44,45], while their effectiveness in cancer therapy may strongly depends on their ability of EVs to target the tumor tissue: however, despite intense research in the field, still little is known about their *in vivo* biodistribution [35,46–49].

ACCEPTED MANUSCRIPT

Herein, by using a mouse cancer cell line grown in an immunocompetent syngeneic NFκB-*luc2* reporter mouse model and a fluorescent dye to track EVs [35], we took advantage of *in vivo* and *ex vivo* imaging technologies to evaluate, at the same time, the biodistribution and the effects of EV-formulations carrying OVs and/or paclitaxel (PTX) on the immune system. We found that EVs enhanced the systemic delivery of anticancer agents resulting in an improved tumor-selective delivery, peritumoral immune-response associated with the targeted delivery of the virus, enhanced immunogenicity and infiltration of CD4+ and CD8+ T-cells.

MATERIALS AND METHODS

Cell culture

LL/2 mouse lung cancer cell line was purchased from the American Type Culture Collection (ATCC, USA). The cells were cultured at 37 °C and 5 % CO_2 in Dulbecco's modified eagle medium (DMEM, Lonza, Switzerland) supplemented with 10 % fetal bovine serum (FBS, Gibco Laboratories, USA), 1 % of 100 u/mL penicillin/streptomycin (Gibco Laboratories) and 1% L-glutamine (Gibco Laboratories).

Oncolytic virus

The construction and characterization of Ad5D24-CpG has been described previously [50] by recombining a CpG-rich shuttle plasmid (pTHSN-CpG1) with a plasmid containing the 24 adenovirus backbone. Viral stocks were expanded in human lung cancer cell line A549 and purified on cesium chloride gradients. The viral particle concentration was determined by OD_{260}-reading and standard $TCID_{50}$ (tissue culture infectious dose 50) assay was performed to determine infectious particle titer. Virus was characterized by PCR and restriction enzyme.

Paclitaxel (PTX) solutions

A 50 mM stock solution of Paclitaxel (PTX; Selleck Chemicals) was prepared by dissolving PTX into di-methyl sulfoxide (DMSO) (Sigma- Aldrich). 5 µM PTX-PBS solution was used for *in vitro* studies and 10 µM PTX-PBS solution for *in vivo* studies.

Production of EVs, Lipophilic Dye loaded EVs and EVs formulations

In order to produce EVs 2.6 x 10^6 LL/2 cells were plated into T-175 flask in medium supplemented with 5 % FBS. The FBS growth media was ultra-centrifuged overnight (110 000 x g at 4°C for 18 h, Optima LE-80K ultracentrifuge, rotor type 50.2, Beckman Coulter) to remove EVs present in the serum.

ACCEPTED MANUSCRIPT

EVs were isolated from the conditioned medium using differential centrifugation steps. First the conditioned medium was centrifuged at 500 x g in 4°C for 10 minutes to pellet cells (Allegra X-15R Centrifuge, Beckman Coulter). Then, the supernatant was collected and ultra-centrifuged for 2 h at 100 000 x g in 4°C, using Optima L-80 XP ultra-centrifuge (Beckman Coulter) with rotor SW32Ti (Beckman Coulter). The supernatant was aspirated and EV- containing pellets re-suspended in PBS (Lonza) 100 µL and stored at - 80 °C.

PTX-loaded EVs were prepared as previously described [37,39] by incubating 1×10^8–5×10^9 EVs in 1 mL of 5 µM PTX-PBS solution for *in vitro* samples and 10 µM PTX-PBS solution for *in vivo* samples, for 1 h at 22 °C. Then, the samples were centrifuged at 170000 ×g for 2 h to pellet the EVs. The supernatant containing unbound PTX was removed, and the EV-pellet was washed, suspended it in DPBS and pelletted it again at 170000 ×g.

EVs were loaded with DiD lipohilic dye (EV-DiD) and prepared by incubating $1x10^8$-$5\ x10^9$ EVs for 1 hour at RT with 5 µL of DiD (Biotium) per mL of EV suspension in PBS. Next, the samples were centrifuged at 150 000 x g for 3 h to pellet the EVs. The supernatant containing unbound DiD was removed, and the EV-pellet was washed by suspending it in PBS and pelleting it again at 150 000 x g.

Production of EV-Virus formulations

EV-encapsulated virus (EV-Virus) were produced as previously described [39], 2.6 x 10^6 of LL/2 cells were infected with 10 viral particles/cell of Ad5D24CpG and were cultured at 37 °C and 5 % CO_2. 48 h later when most of the cells were detached from the culture flask, the culture media were collected for EV-Virus isolation using differential centrifugation. First the conditioned medium was centrifuged at 500 x g and 4°C for 10 minutes, to separate the cells (Allegra X-15R Centrifuge, Beckman Coulter). Then, the supernatant containing EV-Virus was collected and ultra-centrifuged for 2 h at 100 000 x g and 4°C, using Optima L-80 XP ultra-centrifuge (Beckman Coulter) with rotor SW32Ti (Beckman Coulter). The supernatant was aspirated and pellets containing EV-Virus re-suspended in PBS 100µL and stored at - 80 °C. EV-Virus samples were incubated in 100 mM NaOH at room temperature for 20 minutes in order to inactivate any free not EV encapsulated virus present. Free virus used as controls was always inactivated for each experiment performed as previously reported [51,52]. Samples were subsequently neutralized by the addition of HCl 0.1 M.

To generate EV-DiD-Virus, the EV-Virus formulation was incubated for 1h at RT in 5 µL of DiD per mL of EV suspension in DPBS. Samples were then centrifuged at 150 000 x g for 3 h at RT, in order to pellet EV-DiD-Virus. The washing procedure was repeated using PBS as diluent. The final EV-DiD-Virus pellet was re-suspended in 100 µL of PBS and stored at -80 °C until use.

ACCEPTED MANUSCRIPT

Size distribution analysis by nanoparticle tracking analysis (NTA)

Size distribution and concentration of EV, EV-PTX, EV-Virus and EV-Virus-PTX formulations were analyzed by NTA using Nanosight model LM14 (Nanosight) equipped with blue (404 nm, 70 mV) laser and sCMOS camera. The samples containing virus were incubated at +95 °C for 10 minutes in order to inactivate the viruses. NTA was performed for each sample by recording three 90 seconds videos, subsequently analyzed using NTA software 3.0 (Nanosight). The detection threshold was set to level 5 and camera level to 15.

Zeta potential analysis by electrophoretic light scattering

The zeta potential was measured using ZetaSizer Nano (Malvern, UK). All the samples were diluted in a volume of 800 μL of MilliQ H_2O and injected with a 1 mL syringe in the capillary flow (DTS1070 folded capillary cell) for the measurement. An equilibration time of 120 seconds was set on the software to allow the samples to stabilize at 25°C inside the measurement chamber. Three parallel measurements were performed on each sample.

Cryo-EM

Cryo-EM images were acquired with a FEI Talos Arctica 200 kV FEG electron microscope equipped with a FEI Falcon 3EC direct electron detector and Volta Phase-plate. Prior to Cryo-EV imaging, samples were vitrified on a FEI Vitrobot IV apparatus, and processed as previously reported [53].

MTS cell viability assay

LL/2 cells were seeded at a density of $1x10^4$ cells/well in 96-well plates and maintained under standard growth condition. On the following day cells were treated in triplicates with control EVs (10 particles/cell), Virus (10vp/cell), PTX (0.1 pmol/cell), Virus and PTX separately (Virus+PTX) (10 vp/cell, 0.1 pmol/cell of PTX), EV-PTX (10 particles/cell, 0.1 pmol/cell of PTX), EV-Virus (10 particles/cell), EV-Virus-PTX (10 particles/cell, 0.1 pmol/cell of PTX). Cell viability was determined by MTS assay according to the manufacturer's protocol (Cell Titer 96 AQueous One Solution Cell Proliferation Assay; Promega, Nacka, Sweden). The absorbance was measured with a 96-wells plate spectrophotometer Varioskan Flash Multimode Reader (Thermo Scientific) at 490 nm. The experiments were independently performed three times with triplicates of each condition in each experiment

Immunogenicity of tumor cell death in vitro

ACCEPTED MANUSCRIPT

Calreticulin (CRT) exposure. Cells were seeded in duplicate onto 6 well plates at $5x10^5$ cells/well. Cells were treated with control EVs (10 particles/cell), Virus (10 vp/cell), Virus and PTX separately (Virus+PTX) (10 vp/cell, 0.1 pmol/cell of PTX), EV-PTX (10 particles/cell, 0.1 pmol/cell of PTX), EV-Virus (10 particles/cell), EV-Virus-PTX (10 particles/cell, 0.1 pmol/cell of PTX). After 24 h cells were harvested and stained with 1:1000 diluted rabbit polyclonal anti-Calreticulin antibody (Abcam, Cambridge, UK) for 40 minutes at 4°C subsequently with 1:100 diluted Alexa-Fluor 488 secondary antibody (Invitrogen, Carlsbad, CA) and analyzed by flow cytometry (LSR II, BD, Franklin Lakes, NJ).

ATP release. Cell lines were seeded in triplicates onto 96 well plates at $1x10^4$ cells/well and treated as mentioned above. Supernatants were collected after 48 h and analyzed with ATP Determination Kit according to manufacturer's protocol (Promega, Madison, WI) for luminometric analysis (Varioscan Flash, ThermoFisher Scientific, Waltham, MA).

In vivo biodistribution study

Day 0 **Day of treatment**	**Day 1** **Detection of intensity of photon emission (BLI)**	**Day 1** **Detection of intensity of photon emission (Fluorescence)**
Vehicle	**X**	
Virus ($1x10^8$ vp/tumor)	**X**	**-**
EV ($1x10^9$ particles/tumor, and 5 µL of DiD per mL of EV suspension)	**X**	**-**
PTX (40µmol of PTX/kg)	**X**	**-**
EV-PTX ($1x10^8$ particles/tumor including $1x10^8$ vp/tumor, and 10 µM of PTX/kg)	**X**	**-**
EV-Virus ($1x10^8$ particles/tumor + $1x10^8$ vp/tumor)	**X**	**EV-DiD-Virus: $1x10^8$ particles/tumor + 0.5 µL of DiD/ tumor + $1x10^8$ vp/tumor**
EV-Virus-PTX ($1x10^8$ particles/tumor including $1x10^8$ vp/tumor and 40µmol of PTX/kg)	**X**	**-**

Table 1. Study design for the *in vivo* biodistribution

ACCEPTED MANUSCRIPT

All the animal experiments were performed and approved by the Italian Ministry of Research and University permission numbers: 12-12-30012012, 547/2015 and controlled by a Departmental panel of experts. The transgenic reporter NFκB-*luc2* mouse was generated and characterized by our group and used for the *in vivo* studies [54]. The acclimatization period was 14 days prior to LL/2 cancer cell injections. Health status of the mice was monitored daily and as soon as signs of pain or distress were evident they were euthanized. For the bioluminescence study where the bioluminescent signal was related with the inflammation state of tissues, murine xenografts were established by injecting $1x10^6$ LL/2 cells s.c. into the neck of 12-week old male mice. The treatment groups were as follows: vehicle (n=5) (100 µL of PBS), EVs (n=5) ($1x10^9$particles/tumor), PTX (n=3) (40 µmol of PTX/kg), EV-Virus (n=5) ($1x10^8$ vp/tumor), EV-PTX (n=5) ($1x10^8$ particles/tumor and 40 µmol of PTX/kg), EV-Virus-PTX (n=5) ($1x10^8$ vp/tumor and 40 µmol of PTX/kg) (Table 1). The aim of the fluorescence study was to have a direct evidence of the specific tropism of EVs encapsulated with oncolytic viruses to the tumor, thus the fluorescent emission of a lipophilic dye (DiD) was related to the particle biodistribution. Therefore, we performed the following treatments: DiD (5 µL per mL of EV suspension in DPBS), EV-DiD-Virus (n=5) ($1x10^8$ particles/tumor + $1x10^8$ vp/tumor). For the bioluminescence and fluorescent studies, treatment groups were administered i.v (100 µl) to mice with tumors (one tumor per mouse about 5 mm in diameter). Brain, tumors, livers and serum from NFκB-*luc2* mouse were collected for quantitative real time PCR (LighCycler 480, Roche, Basel, Switzerland).

In vivo and *ex vivo* imaging

The *in vivo* bioluminescence imaging analysis was carried out at different time points, starting the day before injection of tumor cells, and ending 24 h post EV treatments (i.v.). For the bioluminescence imaging, animals were injected i.p. with 80 mg/kg of luciferin (Beetle Luciferin Potassium Salt; Promega, Madison, WI, USA) 15 minutes prior the imaging session. Then mice were anaesthetized using Isofluorane (Isofluorane-Vet; Merial, Lyon, France) and kept under anesthesia during imaging sessions carried out with the Imaging System (5 minutes for dorsal view and 5 minutes for ventral view) (IVIS Lumina II Quantitative Fluorescent and Bioluminescent Imaging; PerkinElmer, Waltham, MA, USA). Photon emission in selected body areas was measured using the Living Image Software 3.2 (PerkinElmer). For the *ex vivo* imaging mice were treated with luciferin 15 minutes prior euthanasia by cervical dislocation and *ex vivo* imaging of the selected organs was carried out immediately after death. Bioluminescence from tissue explants was acquired over a 5 minutes exposure time and quantified with the Living Image Software 3.2 (PerkinElmer).

ACCEPTED MANUSCRIPT

The *in vivo* fluorescence imaging was carried out 24 h post i.v. EV treatments using the same Imaging System (IVIS Lumina II) with suitable filters (Cy5.5) and following the manufacturer instructions for fluorescence background subtraction. Similarly, to the above-described procedure for bioluminescence imaging, the *ex vivo* imaging acquisition of fluorescence was performed on tissue explants over an exposition time of 1 second. The quantification was done with Living Image Software 3.2 (PerkinElmer).

Quantitative real-time PCR

qPCR for adenovirus E4 copy number was carried out according to the protocol previously described [55] primer FW: 5'-GGA GTG CGC CGA GAC AAC-3', primer RV: 5'-ACT ACG TCC GGC GTT CCA T-3', probe E4: 5'-(6FAM)-TGG CAT GAC ACT ACG ACC AAC ACG ATC T- (TAMRA)-3'[17]. Total DNA was extracted from LL/2 cells 48h post treatment *in vitro* and from resected brains, tumors, livers, blood from NFκB-*luc2* mouse model after 24h post treatment, using the QIAamp DNA Blood Mini Kit (Qiagen, Hilden, Germany) according to manufacturer's protocol. Subsequently isolated DNA was analyzed for adenoviral E4 copy number normalized to murine beta-actin (liver, blood) ((primer FW: 5'-CGA GCG GTT CCG ATG C-3', primer RV: 5'-TGG ATG CCA CAG GAT TCC AT-3', probe murine beta-actin: 5'-(6FAM)-AGG CTC TTT TCC AGC CTT CCT TCT TGG-(TAMRA)-3'. Samples were analyzed using LighCycler qPCR machine (LighCycler 480, Roche, Basel, Switzerland).

Immune cell infiltration analysis

Immune cell infiltration of tumors was analyzed using the flow cytometer BD LSR II (BD Biosciences) and FlowJo software (Tree Star, Ashland, OR, USA) at sacrifice (24h post-treatment). Specific lymphocites were quantified using antibodies CD45+ (Abcam, ab210185), CD3+ (Abcam, ab34275), CD4+ (Abcam, ab210348), CD8+ (Abcam, 25499). Tumors were harvested and weighted. Neoplastic tissues were dissociated with tumor dissociation kit mouse (Miltenyi Biotec 130-096-730). After dissociation, cells were washed and stained with antibodies according to manufacturer's instructions.

Statistical analysis

Statistical significance was analyzed by using one-way ANOVA with Tukey's Multiple Comparison test and nonparametric Mann–Whitney test. All statistical analysis, calculations and tests were

ACCEPTED MANUSCRIPT

performed using GraphPad Prism 5 (GraphPad Software, San Diego, CA).

RESULTS

Production of LL/2-derived EVs formulations and their ability to induce immunogenic cell death

We previously demonstrated that human lung cancer cell-derived EVs could be useful vehicles for the systemic drug delivery of OVs and paclitaxel (PTX) to target and reduce tumor growth in nude mice with compromised immune system [39]. Since, OVs are able to trigger the host anti-tumor immunity actively contributing to their mechanism of action [56,57], in the current study, we aimed at evaluating the effects of EV formulations on the immune system; for testing these effects, we used a mouse lung cancer cell line (LL/2) to produce the EV-formulations (encapsulating PTX and OVs) and to generate a tumor model in immunocompetent syngeneic mice (C57Bl/6). In a first set of experiments, we assessed whether the encapsulation of PTX and OVs into the LL/2-derived EVs had influence on the particle size distribution by using NTA (Figure 1AB). After encapsulation, free viruses remaining in solution were chemically inactivated as previously reported [51,52] and should not have played a significant role in the experiments carried out with the EV-Virus formulations. Size distribution of both control EVs and EV-Virus formulations were detected to be in the range of 50-400 nm. The size distribution of EV-Virus overlapped with the size of the Virus with most of the EVs being smaller or the same size as the virus (Figure 1A). Additionally, no significant size differences were detected by adding PTX in EV-Virus-PTX and EV-PTX (EVs loaded with PTX) (Figure 1B). Indeed, EVs and EV-Virus had a negative zeta-potential of approximately -40 mV, while the free virus had a zeta-potential of -20 mV (Figure 1C). The zeta-potential was also comparable in EV-Virus-PTX and EV-PTX formulations, as PTX is a chargeless molecule (Figure 1C). Cryo-EM experiments showed that virus was incorporated inside the vesicles. The adenovirus virion has a viral structure of 90–100 nm in size packed inside the EV (Figure 1D). Although we rigorously standardized the procedure for the encapsulation of the virus into the EVs, the ratio between free and EV-encapsulated virus could not be systematically determined. The Cryo-EM images demonstrated that the free virus was less frequent compared to the encapsulated virus, but this was only a qualitative observation that for future clinical applications should be firmly determined. Nevertheless, the remaining free virus was routinely inactivated (please, see the procedure in the Material and Methods section) in the EV-Virus formulations before proceeding with the *in vivo* experiments.

ACCEPTED MANUSCRIPT

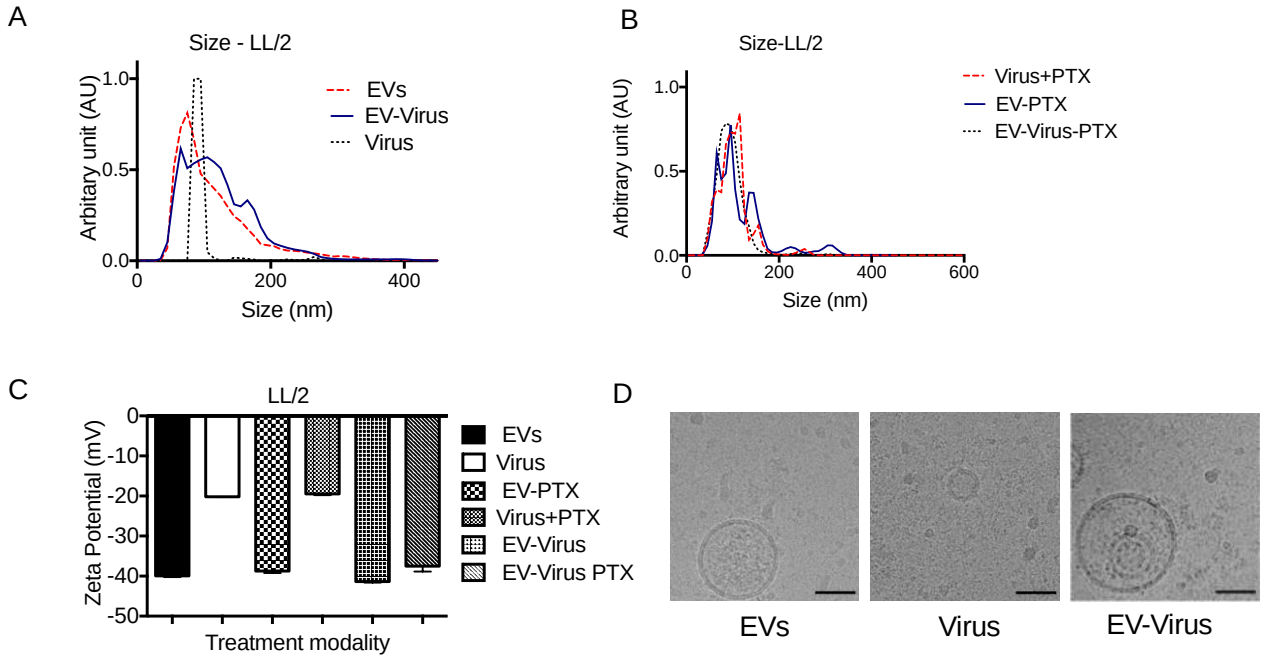

Figure 1. Size and net-charge of murine lung cancer derived extracellular vesicles. (A-B) Size distribution of EVs, EV-Virus,Virus, Virus+PTX, EV-PTX and EV-Virus-PTX samples were determined by using Nano tracking analysis (NTA). (C) The surface charge of the EVs, Virus, EV-PTX, Virus+PTX, EV-Virus and EV-Virus-PTX was measured using ZetaSizer Nano Malvern. (D) Cryo-EM image of EVs, Virus and EV-Virus (scale bar 100 nm) was acquired with a FEI Talos Arctica 200 kV FEG electron microscope equipped with a FEI Falcon 3EC direct electron detector and Volta Phase-plate.

These experiments confirmed that the encapsulation of PTX or OVs had only minimal effects on size and charge of the murine EVs, similarly to what have been observed with formulations obtained with human lung cancer EVs [39]. To gain insights into the anti-tumor activity of the LL/2-derived EVs formulations, we tested their cytotoxic effects on LL/2 cells with the MTS cell viability assay. In keeping with what we have previously reported [39], EV-Virus and EV-Virus-PTX showed enhanced anti-cancer activity when compared to cells treated with the Virus or PTX alone (Figure 2A) ($p<0,001$). To evaluate whether a program of immunogenic cell death was triggered by the treatments, the expression of specific markers, such as the exposure of calreticulin on cell surface and the extracellular release of ATP [58] were measured on murine lung cancer cells treated with EVs (10 particles/cell), Virus (10 vp/cell), PTX (0.1 pmol/cell), Virus and PTX separately (Virus+PTX) (10 vp/cell, 0.1 pmol/cell),), EV-PTX (10 particles/cell, 0.1 pmol/cell), EV-Virus (10 particles/cell), EV-Virus-PTX (10 particles/cell, 0.1 pmol/cell),), PTX (0.1 pmol/cell). The highest immunogenic cell death on tumor cells was observed with Virus+PTX and EV-Virus-PTX treatments (Fig. 2BC), while the EVs administration seemed not influencing either the immunogenic cell death or the viral

ACCEPTED MANUSCRIPT

replication (Fig. 2D); the treatment with PTX slightly decreased viral replication although to a minimal extent (25%). These data suggested that all EV formulations, but not EVs alone, were able to counteract the growth of tumor cells and induce immunogenic cell death.

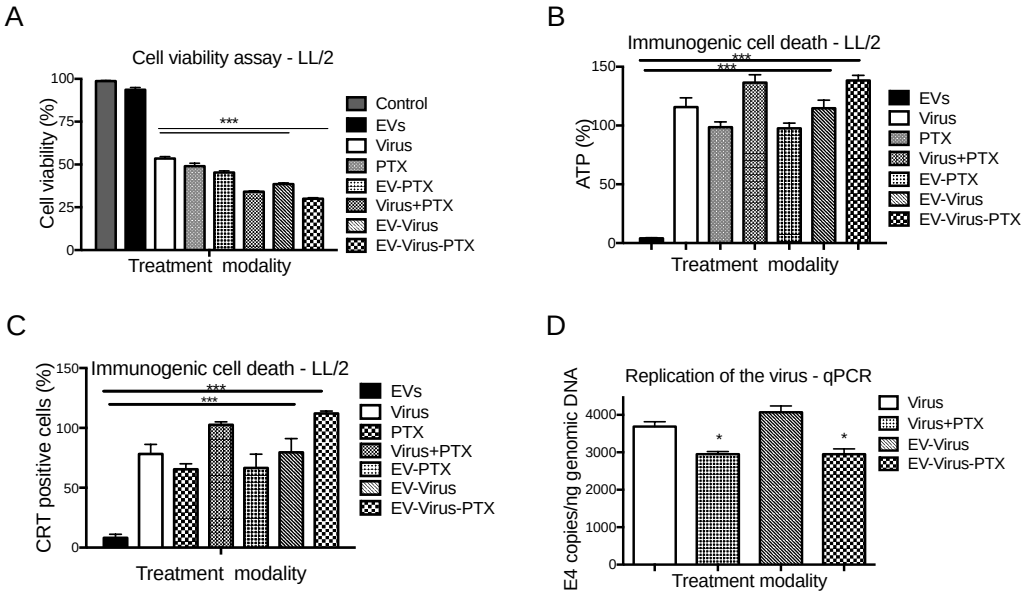

Figure 2. Antitumor properties of extracellular vesicles as drug delivery vehicles. (A) Antineoplastic efficacy was measured by MTS cell viability assay in the LL/2 cell line. Cell viability was determined in untreated cells (control) and 72 h post-treatment. (B) Extracellular ATP was measured from the different supernatants (LL/2 cells) 48h post-treatment using ATP determination kit. (C) Calreticulin exposure on outer cell surface of the murine lung cancer cells was measured 24h post-treatment by flow cytometer. (D) Adenoviral copies towards E4 gene were measured by qPCR from LL/2 cells 24h post-treatment. Error bars mean+/- SD *p<0.05, **p<0.01, ***p<0.001.

Oncolytic viruses encapsulated in EVs induce inflammatory response only in the peritumoral area

The ability of LL/2-derived EV formulations to induce immunogenic cell death *in vitro*, prompted us to verify whether their biodistribution and immunogenic effects were selective for the tumoral tissue *in vivo*. To this aim, we used the NFκB-*luc2* reporter mouse model in which it is possible to monitor in the *spatio*-temporal dimension the activation of the inflammatory pathway in the tissues of living systems [54]. The NFκB-*luc2* model is a mouse genetically engineered with a firefly luciferase reporter gene (*luc2*), whose expression is under the control of an NFκB responsive promoter; in all the reporter mouse tissues (including blood cells), upon activation of the NFκB transcription factor (the master regulator of inflammatory pathways), it is possible to identify the site of inflammation *in vivo* or ex *vivo* by bioluminescence imaging of the luciferase accumulation [54]. The NFκB-*luc2* reporter mouse was transferred into the C57Bl/6 background for the syngeneic engraftment of LL/2 tumor cells. $1x10^6$ LL/2 cells were s.c. injected in the periscapular dorsal area in six groups of five

ACCEPTED MANUSCRIPT

NFκB-Luc2 reporter mice/group to evaluate the inflammatory reaction triggered by the different EV formulations (Figure 3). To this aim, *in vivo* bioluminescence imaging acquisitions were carried out following tumor growth from day -12 (injection of cancer cells) until the tumor reached the dimension of 5 mm, when mice were i.v. treated with the different formulations for 24h (Figure 3 and Table 1); treatments included: vehicle (PBS), Virus, PTX, EV, EV-PTX, EV-Virus and EV-Virus-PTX. Photon emissions were acquired and quantified from the dorsal and ventral sides, to record any increase/decrease of luminescence before and after treatments. The emission from the dorsal area is generally mainly influenced by the tumor area, while from the ventral side, luminescence arises mainly from inner organs (lung, liver, spleen, intestine etc.). The photon emission significantly increased in the tumor area especially in mice treated with Virus, EV-Virus, EV- Virus-PTX (Figure 3 CDE) as compared to the vehicle-treated mice (Figure 3A), while it was only slightly increased in mice treated with EV and EV- PTX (Figure 3BF). These results suggested that the treatments with Virus alone, EV-Virus, EV-Virus-PTX induced an enhanced NFkB dependent inflammatory response only in the peritumoral area (Figure 3AF). From the ventral side, bioluminescence only slightly increased in abdominal (Supplementary Figure 1), hepatic (Supplementary Figure 2) and chest (Supplementary Figure 3) areas following the lung tumor growth and was not dependent from the administered treatment, with the exception of PTX where a systemic inflammatory reaction was observed (Supplementary Figure 4). From these data, we concluded that systemic treatments with Virus, EV-Virus, EV-Virus-PTX selectively induced a tumor-associated inflammation, in line with the tumor-specificity of the virus, suggesting that EVs not only protect viral particles from the host immune system [59,60], but does not trigger *per se* any systemic inflammatory reaction.

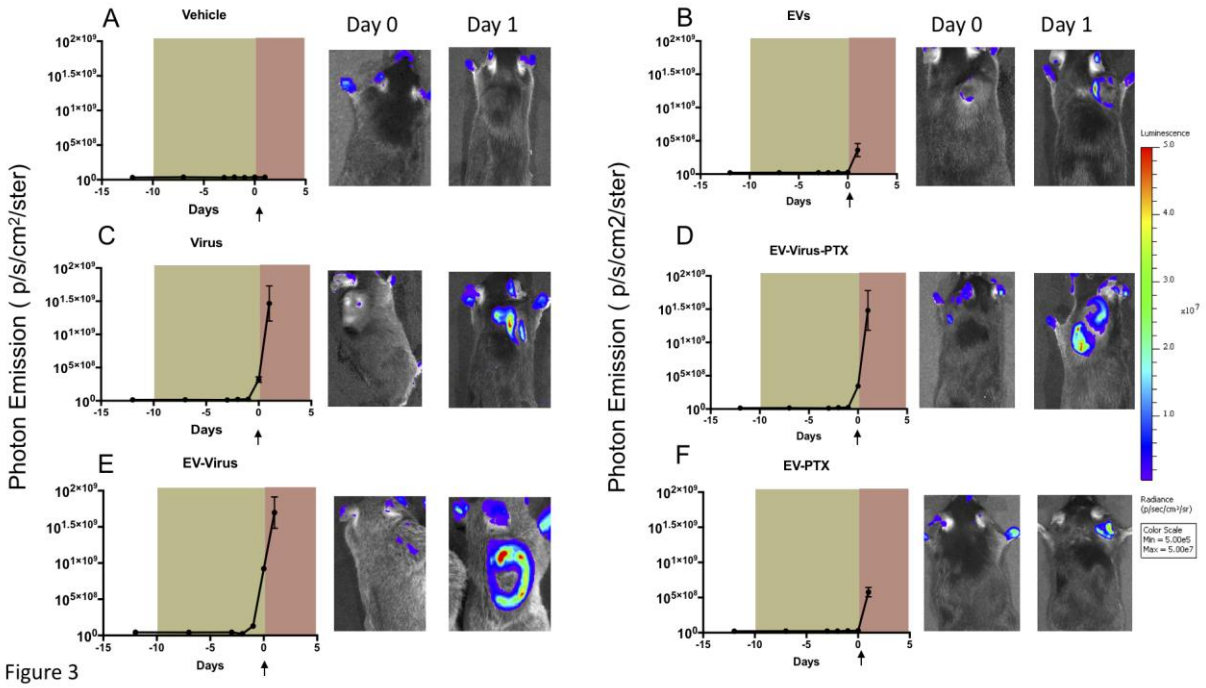

Figure 3

ACCEPTED MANUSCRIPT

Figure 3. EV-formulations induces tumor associated inflammation in NFKB-*luc2* mice. (A-F) Quantification of the photon emission in the tumor areas at the indicated time points. At day 0 mice were treated with the indicated formulations. The tumor cells were injected at day -12. Data are expressed as BLI, average radiance (p/s/cm^2/sr), mean ± SEM (N=5).

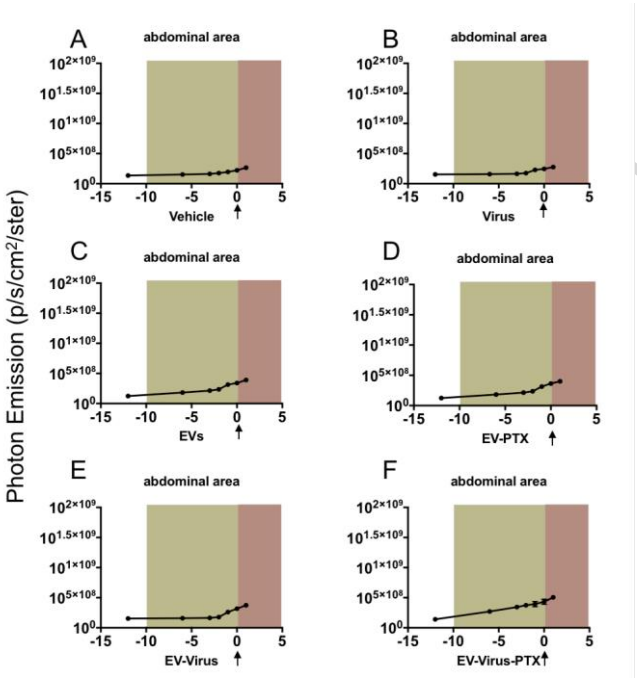

Supplementary Figure 1. Tumor growth induces a generalized inflammatory reaction in the abdominal area. (A-F) Quantification of the photon emission in abdominal area at indicated time point. At day 0 mice were treated with the indicated formulations. Tumor cells were injected at day -12. Data are expressed as BLI, average radiance (p/s/cm^2/sr), mean ± SEM (N=5).

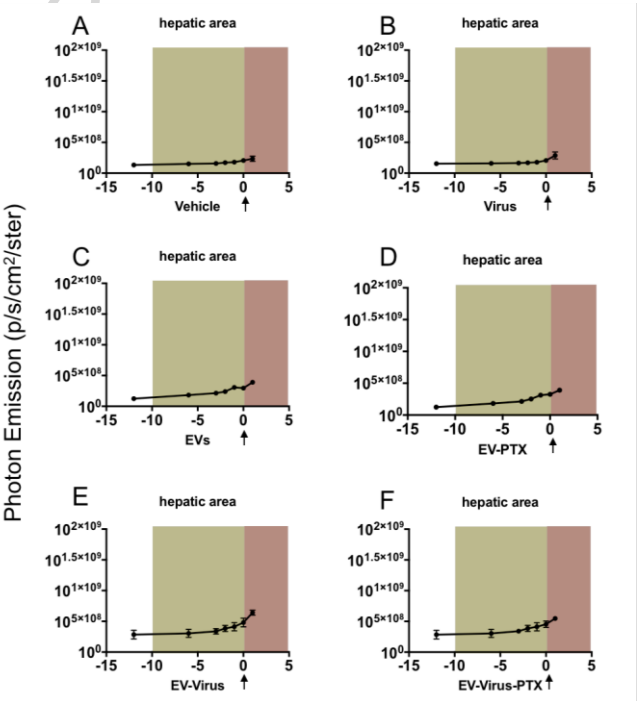

ACCEPTED MANUSCRIPT

Supplementary Figure 2. Tumor growth induces a generalized inflammatory reaction in hepatic area. (A-F) Quantification of the photon emission in hepatic area at indicated time point. At day 0 mice were treated with the indicated formulations. The tumor cells were injected at day -12. Data are expressed as BLI, average radiance (p/s/cm^2/sr), mean ± SEM (N=5).

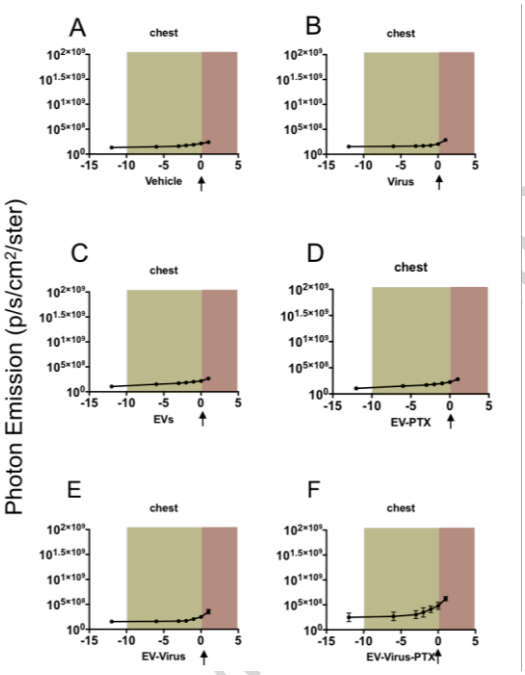

Supplementary Figure 3. Tumor growth induces a generalized inflammatory reaction in chest. (A-F) Quantification of the photon emission in cheast area at indicated time point. At day 0 mice were treated with the indicated formulations. The tumor cells were injected at day -12. Data are expressed as BLI, average radiance (p/s/cm^2/sr), mean ± SEM (N=5).

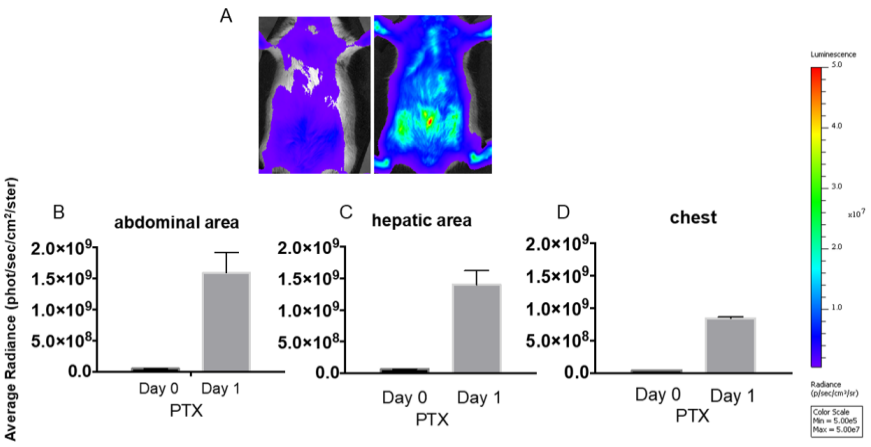

Supplementary Figure 4. Systemic inflammation induced by treatment with paclitaxel. Paclitaxel treatment of NFKB-*luc2* mice induces systemic activation of the NFkB-mediated transcription. (A-D) Quantification of the photon emission in the abdominal, hepatic and chest areas at the indicated time point. Day 0 is the day of paclitaxel administration (i.v.). Data are expressed as BLI, average radiance (p/s/cm^2/sr), mean ± SEM (N=3).

ACCEPTED MANUSCRIPT

To confirm that the BLI photon emission observed *in vivo* was due to the induction of a tumor-associated inflammation and not from other body areas, mice were sacrificed 24 h after treatment and photon emission was measured *ex vivo* in specific organs. The 24h time point was chosen since preliminary time course experiments demonstrated that PTX and EV-PTX formulations were inducing NFkB transcription as early as 6 h after treatment (Supplementary Figure 5); thus 24 h was considered a sufficient time length to measure any residual PTX activity eventually distributing to organs other than the tumor. The intensity of photon emission showed that treatments with Virus alone, EV, EV-PTX, EV-Virus, EV-Virus-PTX were associated with inflammation at the tumor site (Figure 4ACDFGH) and not in any other organ; indeed, vehicle alone did not increase bioluminescence in the tumor at this stage of cancer growth (Figure 4 AB). Interestingly, PTX alone induced a systemic inflammation detectable in all organs tested that was clearly prevented by the EV encapsulation, indicating that EVs are indeed able to prevent the drug delivery to any other organs but the tumor (Figure 4AE).

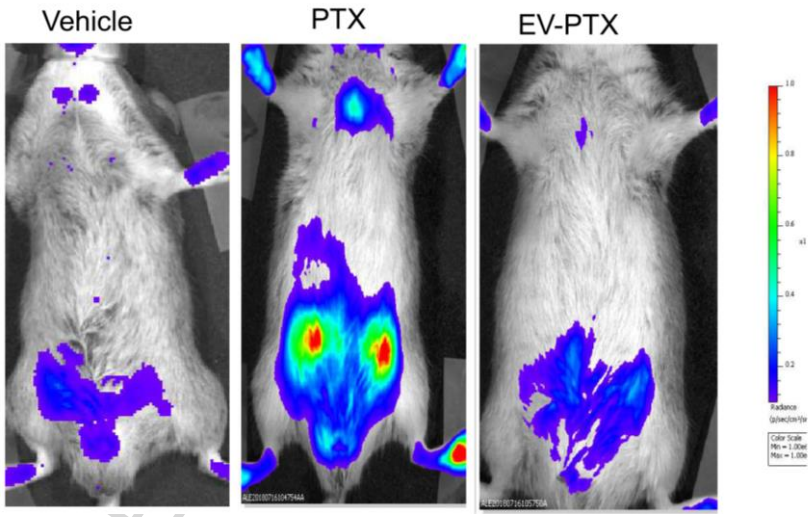

Supplementary Figure 5. In vivo bioluminescence of PTX and EV-PTX after 6h post-treatment. PTX and EV-PTX treatments show the induction of NFkB transcription 6 h after treatment

ACCEPTED MANUSCRIPT

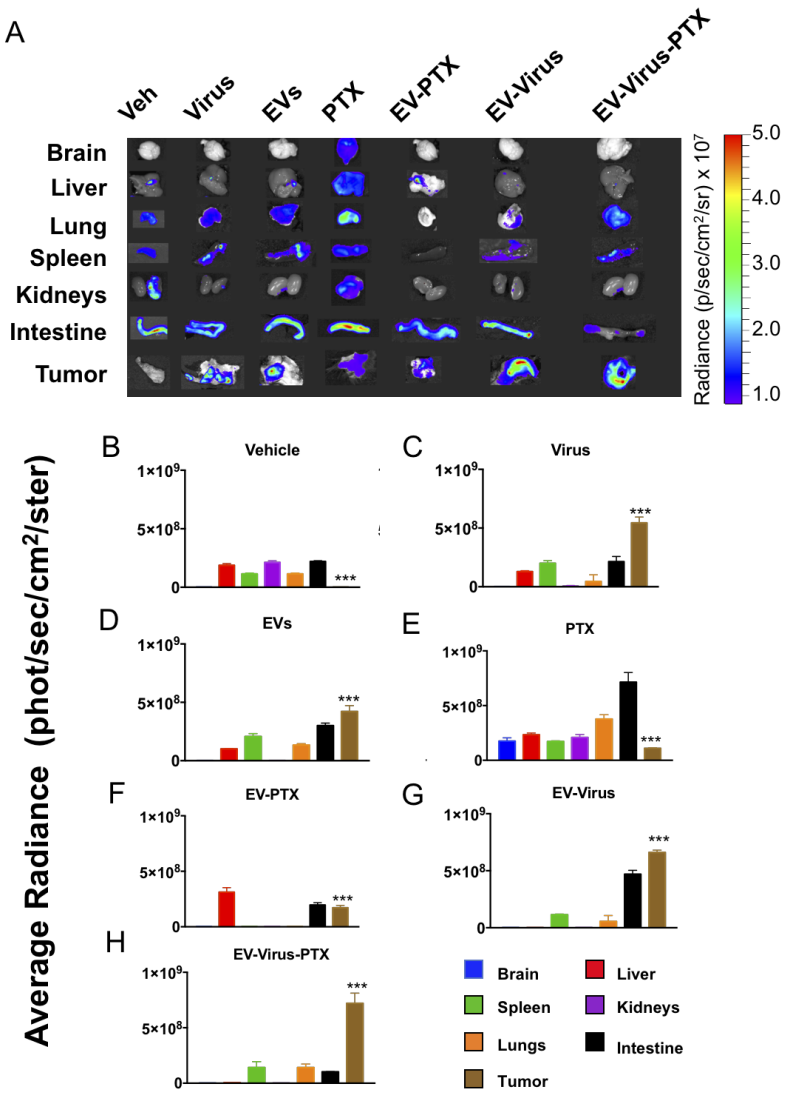

Figure 4

Figure 4. ***Ex vivo*** **bioluminescence is related to the induction of tumor associated inflammation.** (A) Representative images that indicate the intensity of photon emission in organs explanted from NFKB-*luc2*. (B-H) Quantification of the photon emission from 7 indicated organs (brain, liver, spleen, kidneys, lung, intestine, tumor) dissected from NFKB-*luc2* mice 24h after i.v treatments. Data are expressed as BLI, average radiance (p/s/cm^2/sr), mean ± SEM (N=5).

Fluorescent labeling of EVs show a targeted delivery to the tumor site following systemic administration

The ability of EV encapsulation to prevent the systemic inflammation induced by PTX administered alone, clearly suggested that EVs might have a specific tropism for the tumor compared to other body districts. In order to have a direct evidence of this specific targeting, we added to the formulation of EV-Virus (EV-DID-Virus) the fluorescent dye DiIC18(5); 1,1′-dioctadecyl-3,3,3′,3′-

ACCEPTED MANUSCRIPT

tetramethylindodicarbocyanine, 4-chlorobenzenesulfonate salt (DID) that is often used for *in vivo* applications for its high tissue penetrance and low interference with tissue autofluorescence [35,48,61]; then, we evaluated the biodistribution of the fluorescence after i.v. treatment with $1x10^8$ particles/tumor of EV-DID-Virus. The *in vivo* imaging acquisitions of fluorescence and bioluminescence were carried out 24h post-treatment (Figure 5A). The fluorescence imaging showed a specific signal arising from the tumor, thus providing a direct demonstration of the homing of the EV-DID-Virus particles to the neoplastic tissue. This cancer-specific targeting induced, the development of a peritumoral immune-response within 24 h (Figure 4B), which was visible in the reporter animals as a bioluminescent emission surrounding the tumor mass (Figure 5A). The immune-response was specifically associated with the targeted delivery of the Virus to the tumor site, since the bioluminescence signal was not observed in the mice treated with EVs alone (Figure 4B). The *ex vivo* imaging analysis of the fluorescence emission from the dissected organs showed a positive signal mostly within the tumor and the liver (Figure 5B). This high *ex vivo* fluorescence in the liver is possibly due to the accumulation of free DiD released by the EVs following the injection, while the i.v. administration of the dye produced a preferential accumulation of the fluorescence in this organ (Supplementary Figure 6). In agreement with this conclusion, the quantification of the viral load by RT-PCR did not provide evidence of the presence of viral particles in the liver, where we found levels comparable with those measured in samples used as negative controls, such as the brain and serum; in contrast, as expected, a very high titer was detected in the tumor (Figure 6A). By changing the scale of fluorescence of three orders of magnitude, minor distribution could be detected also in other tissues mainly spleen, brain, kidneys, lungs and intestine, although these signals were lower than those detected in the tumor (Supplementary Figure 7). The higher signal in spleen (among the lowers) is in agreement with previous reports with other nanoparticles showing a preferential uptake in the spleen; this phenomena might be less evident in our experiments because of the tumor tropism of EVs.

ACCEPTED MANUSCRIPT

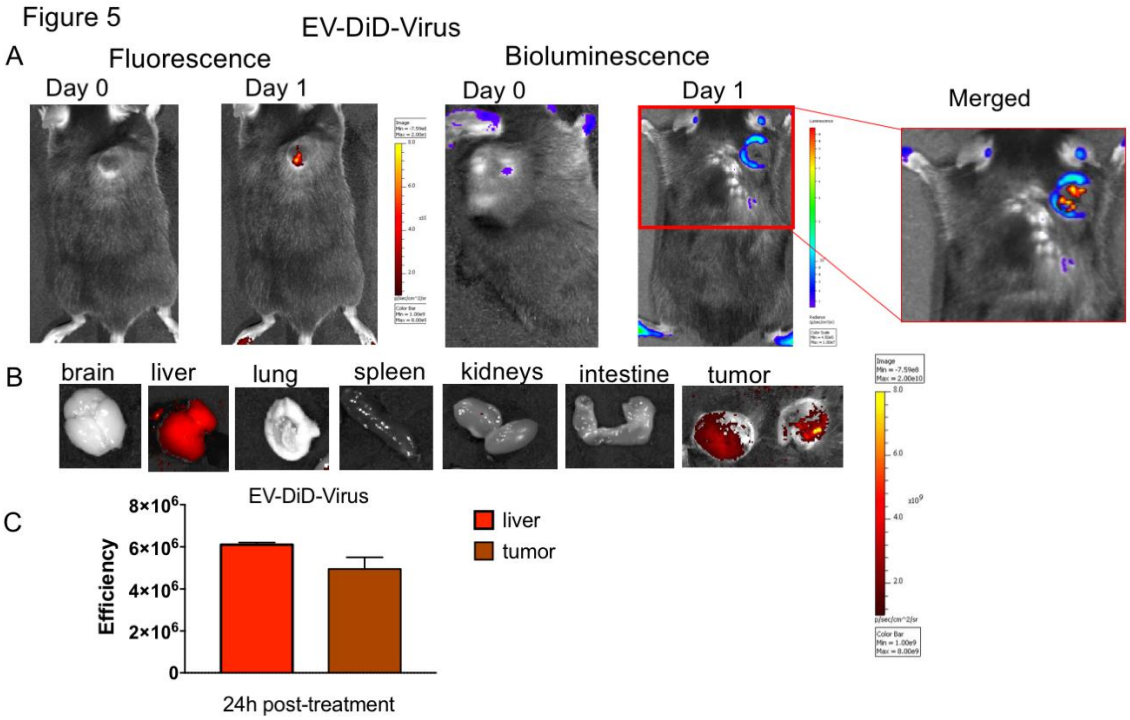

Figure 5. Extracellular vesicles loaded with oncolytic viruses show positive fluorescent signal at the tumor site. (A) Representative images of the photon emission (BLI and fluorescence) in the tumor area of tumor-bearing NFKB-*luc2* mice that were intravenously injected with EV-DiD-Virus ($1x10^8$ particles/tumor + $1x10^8$ vp/tumor). (B) Representative images that indicate the intensity of photon emission in 7 organs explanted from NFKB-luc2 i.v. treated with EV-DiD-Virus. (C) Quantification of fluorescence emission was assessed from liver and tumor tissue using the Living Image Software (PerkinElmer) and CCD-camera (IVIS Lumina II Quantitative Fluorescent and Bioluminescent Imaging; PerkinElmer, Waltham, MA, USA).

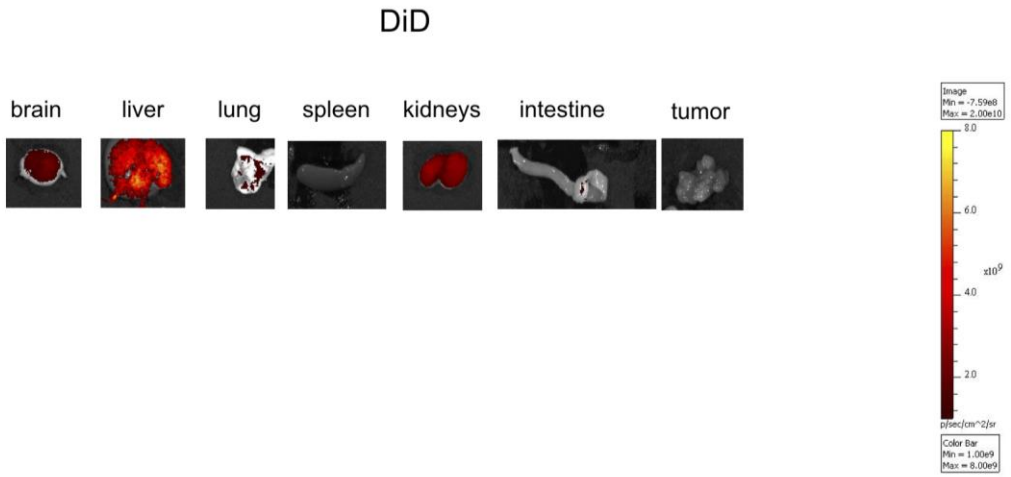

.

ACCEPTED MANUSCRIPT

Supplementary Figure 6. DiD alone does not show positive fluorescent signal in the tumor site. (B) Representative images that indicate the intensity of photon emission in 7 organs explanted from NFKB-luc2 iv treated with DiD.

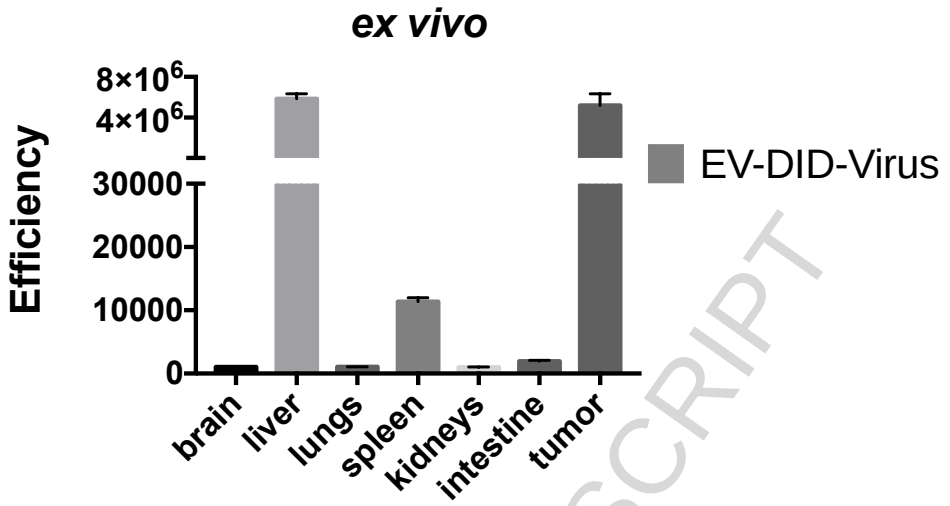

Supplementary Figure 7. *Ex vivo* fluorescence in murine body areas. Quantification of fluorescence emission was assessed using the Living Image Software (PerkinElmer) and CCD-camera (IVIS Lumina II Quantitative Fluorescent and Bioluminescent Imaging; PerkinElmer, Waltham, MA, USA).

Peritumoral infiltration of TILs induced by oncolytic viruses is unaffected by EVs

Next, we analyzed whether the type of inflammatory response recruited by the OVs [62], could be influenced by the delivery of the virus *via* EVs. To this aim, the immune cells infiltrating the resected tumors were analyzed by flow cytometry at sacrifice, 24h post-treatment; the amount of murine CD45+ (pan-leucocyte marker) was initially quantified (Figure 6B) and then the proportion of murine CD3+ T-cells among CD45+ leukocytes was calculated: the data indicated that there was a trend to increase of the CD3+ cell type in the Virus, EV-Virus and EV-Virus-PTX groups (Figure 6C). Similar data were obtained for the subpopulation of CD4+ and CD8+ T-cells displaying a non-significant increased infiltration in the same treatment groups (Figure 6DE). Therefore, we concluded that OVs alone or EV encapsulated with other drugs might enhance immunogenicity; although the significance of this observation has to be firmly established in future studies, we could conclude that the encapsulation of virus into EVs was not interfering with the observed immunogenic response.

ACCEPTED MANUSCRIPT

Figure 6

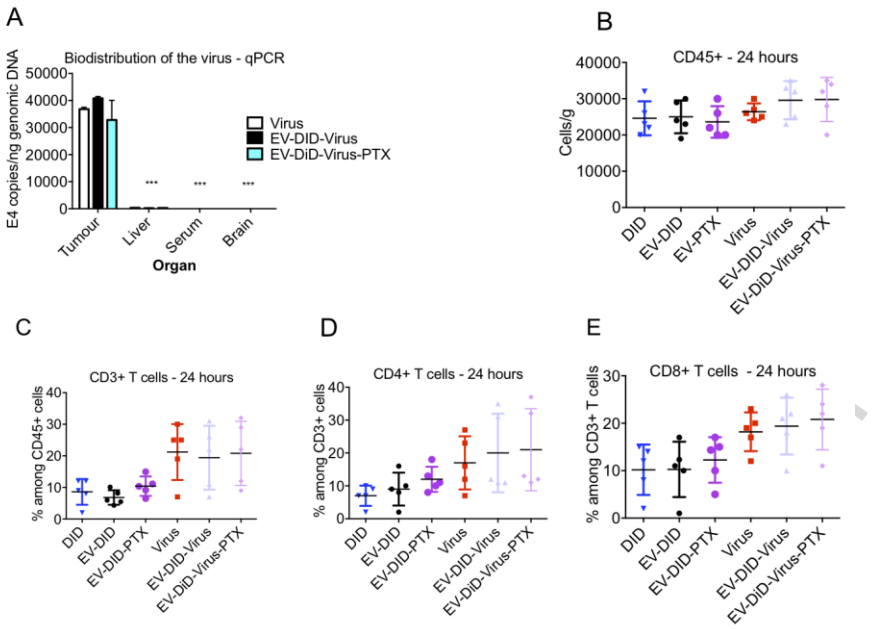

Figure 6. Biodistribution of virus and immune cell infiltration. (A) Adenoviral copies towards E4 gene were measured by qPCR from euthanized mice's organs (tumor, liver, serum and brain) at the end of the treatment. Error bars mean+/- SD *p<0.05, **p<0.01, ***p<0.001. (B-E) % of murine CD45+, CD3+, CD4+, CD8+ T-cells was quantified from resected tumors by flow cytometer. Results are presented as mean +/- SD. N=5/group. One-way ANOVA analysis did not evidence statistical differences between the tested groups.

DISCUSSION

The use of EVs as delivery system of OVs [39,63] or anti-neoplastic drugs [37,64] is a promising therapeutic strategy for primary and metastatic cancers. Nevertheless, the EVs biodistribution profile [65] and the potential side-effects associated with the systemic administration of OVs encapsulated in EVs are still poorly characterized. We have previously developed a strategy to encapsulate in EVs anti-cancer agents, including OVs and PTX together, showing, for the first time, that these formulations can be administered systemically: we reported a selective cancer cell tropism along with inhibition of cancer cell growth in nude mice, thus exploiting their potential use of these novel therapeutic concept also for the treatment of metastatic cancers [39]. In the current study, by using an immunocompetent reporter mouse model (NFkB-luc2), we aimed at assessing the effects of the intravenous delivery of these EVs formulations on the systemic and tumor-associated inflammation.

In fact, although extensive studies have been conducted to demonstrate their potential as drug delivery vessels [34,38,66–69], still little is known about the possible immunogenic or potential toxic effects of EVs [70]. This is especially important given that some of the EV cargo may carry toxic

ACCEPTED MANUSCRIPT

constituents or may instigate inflammatory responses [70–72]. Our *in vivo* imaging evidence on EVs biodistribution clearly show a targeted delivery of the particles selectively to the tumor tissues: we found that the systemic effects of PTX resulting in a diffuse inflammatory reaction, were efficiently reduced by encapsulating the drug inside EVs (Figure 4AF). This is a promising result showing that the potential toxic and inflammatory effects of PTX on the whole body can be prevented by the ability of the nanoparticles to specifically target the tumor tissue. In addition, it has been previously reported that EVs may release mediators of the immune response, such as interleukin (IL)-1β [73–75], IL-18 [76], IL-8 [77], lipid mediators [78,79], matrix metalloproteinases [80] and miRNAs such as let-7, miRNA-21, and miR-29a [81,82], nevertheless, our *in vivo* imaging data clearly indicate that no systemic reaction could be detected other than the tumor associated inflammation.

It is well-known that tumor-associated inflammation may have positive or negative effects depending on the type of the produced immune response [83]: while cytotoxic response is essential for tumor cell removal from the body [84], the response associated with tissue repair may promote invasion and angiogenesis through the secretion of specific growth factors and cytokines [85,86]. The ability of oncolytic adenovirus ONCOS-102 to elicit immune-activation has been already reported in phase I clinical study, showing short-term increase in systemic pro-inflammatory cytokines, a prominent infiltration of TILs in tumors post-treatment (11 out of 12 patients) and systemic induction of tumor-specific CD8+ T cells (2 patients) [26]. Hence, oncolytic therapy does not only kill cancer cells by direct lysis, but also generate antitumor immune responses, long- lasting cancer control and tumor reduction [87]. We found that the systemic administration of OVs encapsulated in EVs enhances immunogenicity of cancer cell death *in vitro* and resulted in infiltration of CD3+, CD4+ and CD8+ T-cells into tumors. Moreover, we demonstrated that EV formulations does not negatively influence the cytotoxic tumor-associated response induced by the treatment with OVs (in terms of inflammatory cell infiltrates). Taken together, these results may suggest an enhanced cytotoxic immune effect at the tumor site induced by OVs when encapsulated in EVs; certainly, the impact of these effects have to be further investigated in long-lasting experiments focusing on anti-tumor efficacy, but this was not the primary aim of this work. In addition, encapsulating OVs inside the EVs may also have the added value to allow the virus to escape from immune-surveillance, making it less detectable and thus likely more effective.

Despite these potential advantages in using EVs as drug delivery tools, there are still some challenges to overcome for its clinical application. Currently there are no universal protocols for EV production, as carriers for drug delivery, thus a standardized protocol should be developed in the near future [88]. Indeed, the low production yield of EVs together with their short half-life, after i.v. administration, is a big hurdle that need to be beaten [66,88–90] before their application for clinical purposes. It has

ACCEPTED MANUSCRIPT

been reported that some cancer cell-derived EVs have a nano-filamentous network, which facilitates interaction with the cell membrane and increases the EV-uptake [67]. These characteristics could possibly be considered for improvements in the design of efficient EV-based drug carriers to be used in cancer therapy [91]. Future studies should take advantage of the EVs pseudo-typing to improve specificity and to drive their tropism towards specific cancers. For instance, EVs expressing Integrin alpha V beta 5 ($ITGa_Vb5$), bind specifically to Kupffer cells, mediating liver tropism, while other integrins $ITGa_6b4$ and ITGa6b1 on EVs bind to lung-resident fibroblasts and epithelial cells, leading to lung tropism [92]. Therefore, by specific modifications of $ITGa_Vb5$, the tropism of EVs could be changed. The pseudotyped EVs combined with the last generation OVs carrying genetic modifications for a cancer-cell restricted replication, may further reduce the potential off-target effects linked to the systemic delivery. The final goal is to exploit the OVs specific oncolytic and immunomodulatory activities and combine them with anti-cancer properties of currently available drugs for an EV-driven, highly effective treatment.

CONCLUSION

In this study, we supported EVs as a tool for systemic delivery of anticancer agents alone or in a combination therapy. We demonstrated the ability of EVs to selectively deliver anti-neoplastic agents to the tumor tissue, thus, potentially reducing the systemic effect of chemotherapy. Moreover, we showed that encapsulation into EVs does not change the ability of OVs to stimulate a tumor-associated inflammatory response in terms of NFκB stimulation, enhanced immunogenicity and infiltration of CD3+, CD4+ and CD8+ T-cells. Altogether, our experiments strongly support the systemic administration of anticancer agent combinations encapsulated into EVs as a novel, safe and efficacious therapeutic strategy aimed at treating primary and metastatic cancers.

Acknowledgments

Funding by MIUR (Departments of excellence Italian Law n.232, 11th December 2016) (V.M, P.C). Financial support by grants from Post doc pool foundation (016947- 3) (M.G.), Italian Association for Cancer Research grant IG-11903 (P.C.), MINIATURA 2 (2018/02/X/NZ7/00727) funded by National Science Center (L.K)

ACCEPTED MANUSCRIPT

REFERENCES

[1] R. Siegel, K. Miller, A. Jemal, Cancer statistics , 2015 ., CA Cancer J Clin. 65 (2015) 29. doi:10.3322/caac.21254.

[2] J.D.M.P. Charles G.Drake Elizabeth, Mechanisms of Immune Evasion by Tumors, Adv. Immunol. 90 (2006) 51–81.

[3] R. Hendrickx, N. Stichling, J. Koelen, L. Kuryk, A. Lipiec, U.F. Greber, Innate Immunity to Adenovirus, Hum. Gene Ther. 25 (2014) 265–284. doi:10.1089/hum.2014.001.

[4] A. Howells, G. Marelli, N.R. Lemoine, Y. Wang, Oncolytic Viruses—Interaction of Virus and Tumor Cells in the Battle to Eliminate Cancer, Front. Oncol. 7 (2017). doi:10.3389/fonc.2017.00195.

[5] C. Capasso, A. Magarkar, V. Cervera-carrascon, M. Fusciello, S. Feola, M. Muller, A novel in silico framework to improve MHC-I epitopes and break the tolerance to melanoma, 6 (2017).

[6] A. Swaika, W.A. Hammond, R.W. Joseph, Current state of anti-PD-L1 and anti-PD-1 agents in cancer therapy, Mol. Immunol. 67 (2015) 4–17. doi:10.1016/J.MOLIMM.2015.02.009.

[7] C.Y.& T.S. Veronika Groh, Jennifer Wu, Tumour-derived soluble MIC ligands impair expression of NKG2D and T-cell activation, Nature. 419 (2002) 734–738.

[8] V. Groh, K. Smythe, Z. Dai, T. Spies, Fas ligand–mediated paracrine T cell regulation by the receptor NKG2D in tumor immunity, Nat. Immunol. 7 (2006) 755. http://dx.doi.org/10.1038/ni1350.

[9] L. Kuryk, A.-S.W. Møller, M. Jaderberg, Quantification and functional evaluation of CD40L production from the adenovirus vector ONCOS-401, Cancer Gene Ther. (2018). doi:10.1038/s41417-018-0038-x.

[10] R.B. Mokhtari, T.S. Homayouni, N. Baluch, E. Morgatskaya, S. Kumar, B. Das, H. Yeger, Combination therapy in combating cancer, Oncotarget. 8 (2015) 38022–38043. doi:10.18632/oncotarget.16723.

[11] N.E. Papaioannou, O. V. Beniata, P. Vitsos, O. Tsitsilonis, P. Samara, Harnessing the immune system to improve cancer therapy, Ann. Transl. Med. 4 (2016) 261–261. doi:10.21037/atm.2016.04.01.

[12] L. Kuryk, A.-S.W. Møller, M. Jaderberg, Combination of immunogenic oncolytic adenovirus ONCOS-102 with anti-PD-1 pembrolizumab exhibits synergistic antitumor effect in humanized A2058 melanoma huNOG mouse model, Oncoimmunology. 00 (2018) 1–11. doi:10.1080/2162402X.2018.1532763.

[13] B. Iovine, M. Garofalo, M. Orefice, V. Giannini, F. Gasparri, G. Monfrecola, M.A.

ACCEPTED MANUSCRIPT

Bevilacqua, Isoflavones in aglycone solution enhance ultraviolet B-induced DNA damage repair efficiency, Clin. Exp. Dermatol. 39 (2014) 391–394. doi:10.1111/ced.12290.

[14] B. Iovine, M. Garofalo, M. Orefice, M.A. Bevilacqua, CHAPTER 21 l-Carnosine and Human Colon Cancer, in: Imidazole Dipeptides Chem. Anal. Funct. Eff., The Royal Society of Chemistry, 2015: pp. 393–411. doi:10.1039/9781782622611-00393.

[15] M. Murtaza, S.J. Dawson, D.W.Y. Tsui, D. Gale, T. Forshew, A.M. Piskorz, C. Parkinson, S.F. Chin, Z. Kingsbury, A.S.C. Wong, F. Marass, S. Humphray, J. Hadfield, D. Bentley, T.M. Chin, J.D. Brenton, C. Caldas, N. Rosenfeld, Non-invasive analysis of acquired resistance to cancer therapy by sequencing of plasma DNA, Nature. 497 (2013) 108–112. doi:10.1038/nature12065.

[16] E.K. Park, K. Takahashi, T. Hoshuyama, T.J. Cheng, V. Delgermaa, G.V. Le, T. Sorahan, Global magnitude of reported and unreported mesothelioma, Environ. Health Perspect. 119 (2011) 514–518. doi:10.1289/ehp.1002845.

[17] L. Kuryk, E. Haavisto, M. Garofalo, C. Capasso, M. Hirvinen, S. Pesonen, T. Ranki, L. Vassilev, V. Cerullo, Synergistic anti-tumor efficacy of immunogenic adenovirus ONCOS-102 (Ad5/3-D24-GM-CSF) and standard of care chemotherapy in preclinical mesothelioma model, Int. J. Cancer. 139 (2016) 1883–1893. doi:10.1002/ijc.30228.

[18] M. Garofalo, B. Iovine, L. Kuryk, C. Capasso, M. Hirvinen, A. Vitale, M. Yliperttula, M.A. Bevilacqua, V. Cerullo, Oncolytic Adenovirus Loaded with L-carnosine as Novel Strategy to Enhance the Antitumor Activity, Mol. Cancer Ther. 15 (2016) 651–660. doi:10.1158/1535-7163.MCT-15-0559.

[19] M. Hirvinen, C. Capasso, K. Guse, M. Garofalo, A. Vitale, M. Ahonen, L. Kuryk, M. Vähä-Koskela, A. Hemminki, V. Fortino, D. Greco, V. Cerullo, Expression of DAI by an oncolytic vaccinia virus boosts the immunogenicity of the virus and enhances antitumor immunity, Mol. Ther. - Oncolytics. 3 (2016) 1–9. doi:10.1038/mto.2016.2.

[20] L. Kuryk, L. Vassilev, T. Ranki, A. Hemminki, A. Karioja-Kallio, O. Levälampi, A. Vuolanto, V. Cerullo, S. Pesonen, Toxicological and bio-distribution profile of a GM-CSF-expressing, double-targeted, chimeric oncolytic adenovirus ONCOS-102 – Support for clinical studies on advanced cancer treatment, PLoS One. 12 (2017) 1–15. doi:10.1371/journal.pone.0182715.

[21] I. Diaconu, V. Cerullo, M.L.M. Hirvinen, S. Escutenaire, M. Ugolini, S.K. Pesonen, S. Bramante, S. Parviainen, A. Kanerva, A.S.I. Loskog, A.G. Eliopoulos, S. Pesonen, A. Hemminki, Immune response is an important aspect of the antitumor effect produced by a CD40L-encoding oncolytic adenovirus, Cancer Res. 72 (2012) 2327–2338. doi:10.1158/0008-5472.CAN-11-2975.

ACCEPTED MANUSCRIPT

[22] C. Capasso, M. Hirvinen, M. Garofalo, D. Romaniuk, L. Kuryk, T. Sarvela, A. Vitale, M. Antopolsky, A. Magarkar, T. Viitala, T. Suutari, A. Bunker, M. Yliperttula, A. Urtti, V. Cerullo, Oncolytic adenoviruses coated with MHC-I tumor epitopes for a new oncolytic vaccine platform, J. Immunother. Cancer. 3 (2015) P333. doi:10.1186/2051-1426-3-S2-P333.

[23] Ł. Kuryk, M. Wieczorek, S. Diedrich, S. Böttcher, A. Witek, B. Litwińska, Genetic analysis of poliovirus strains isolated from sewage in Poland, J. Med. Virol. 86 (n.d.) 1243–1248. doi:10.1002/jmv.23803.

[24] D.Y. Sze, T.R. Reid, S.C. Rose, Oncolytic virotherapy, J. Vasc. Interv. Radiol. 24 (2013) 1115–1122. doi:10.1016/j.jvir.2013.05.040.

[25] J.C. Russell, Stephen J; Peng, Kah-Whye and Bell, Oncolytic Virotherapy, Nat. Biotechnol. 30 (2012) 658–670. doi:10.1038/nbt.2287.ONCOLYTIC.

[26] T. Ranki, S. Pesonen, A. Hemminki, K. Partanen, K. Kairemo, T. Alanko, J. Lundin, N. Linder, R. Turkki, A. Ristimï¿½ki, E. Jï¿½ger, J. Karbach, C. Wahle, M. Kankainen, C. Backman, M. von Euler, E. Haavisto, T. Hakonen, R. Heiskanen, M. Jaderberg, J. Juhila, P. Priha, L. Suoranta, L. Vassilev, A. Vuolanto, T. Joensuu, Phase I study with ONCOS-102 for the treatment of solid tumors - an evaluation of clinical response and exploratory analyses of immune markers, J. Immunother. Cancer. 4 (2016) 1–18. doi:10.1186/s40425-016-0121-5.

[27] L. Vassilev, T. Ranki, T. Joensuu, E. Jäger, J. Karbach, C. Wahle, K. Partanen, T. Alanko, R. Turkki, N. Linder, J. Lundin, A. Ristimäki, M. Kankainen, M. Jäderberg, P. Priha, A. Vuolanto, S. Pesonen, Repeated intratumoral administration of ONCOS-102 leads to systemic antitumor transcriptional immune activation at tumor site in a patient with ovarian cancer Repeated intratumoral administration of ONCOS-102 leads to systemic antitumor CD8 C T-cell respo, (2016) 6–11. doi:10.1080/2162402X.2015.1017702.

[28] M. Siurala, S. Bramante, L. Vassilev, M. Hirvinen, S. Parviainen, S. Tähtinen, K. Guse, V. Cerullo, A. Kanerva, A. Kipar, M. Vähä-Koskela, A. Hemminki, Oncolytic adenovirus and doxorubicin-based chemotherapy results in synergistic antitumor activity against soft-tissue sarcoma, Int. J. Cancer. 136 (2015) 945–954. doi:10.1002/ijc.29048.

[29] L. Kuryk, E. Haavisto, M. Garofalo, C. Capasso, M. Hirvinen, S. Pesonen, T. Ranki, L. Vassilev, V. Cerullo, 661. Synergistic Anti-Tumor Efficacy of Immunogenic Adenovirus ONCOS-102 and Standard of Care Chemotherapy in Preclinical Mesothelioma Model, Mol. Ther. 24 (2016) S262. doi:10.1016/S1525-0016(16)33469-4.

[30] K. Morrissey, T. Yuraszeck, C.C. Li, Y. Zhang, S. Kasichayanula, Immunotherapy and Novel Combinations in Oncology: Current Landscape, Challenges, and Opportunities, Clin. Transl. Sci. 9 (2016) 89–104. doi:10.1111/cts.12391.

ACCEPTED MANUSCRIPT

[31] S. Farkona, E.P. Diamandis, I.M. Blasutig, Cancer immunotherapy: The beginning of the end of cancer?, BMC Med. 14 (2016) 1–18. doi:10.1186/s12916-016-0623-5.

[32] B.D. Lichty, C.J. Breitbach, D.F. Stojdl, J.C. Bell, Going viral with cancer immunotherapy, Nat. Rev. Cancer. 14 (2014) 559. http://dx.doi.org/10.1038/nrc3770.

[33] L. Aurelian, Oncolytic viruses as immunotherapy: Progress and remaining challenges, Onco. Targets. Ther. 9 (2016) 2627–2637. doi:10.2147/OTT.S63049.

[34] Y. Lee, S. El Andaloussi, M.J.A. Wood, Exosomes and microvesicles: Extracellular vesicles for genetic information transfer and gene therapy, Hum. Mol. Genet. 21 (2012) 125–134. doi:10.1093/hmg/dds317.

[35] O.P.B. Wiklander, J.Z. Nordin, A. O'Loughlin, Y. Gustafsson, G. Corso, I. Mäger, P. Vader, Y. Lee, H. Sork, Y. Seow, N. Heldring, L. Alvarez-Erviti, C.I. Edvard Smith, K. Le Blanc, P. Macchiarini, P. Jungebluth, M.J.A. Wood, S. El Andaloussi, Extracellular vesicle in vivo biodistribution is determined by cell source, route of administration and targeting, J. Extracell. Vesicles. 4 (2015) 1–13. doi:10.3402/jev.v4.26316.

[36] S. EL Andaloussi, I. Mäger, X.O. Breakefield, M.J.A. Wood, Extracellular vesicles: biology and emerging therapeutic opportunities, Nat. Rev. Drug Discov. 12 (2013) 347. http://dx.doi.org/10.1038/nrd3978.

[37] H. Saari, E. Lázaro-Ibáñez, T. Viitala, E. Vuorimaa-Laukkanen, P. Siljander, M. Yliperttula, Microvesicle- and exosome-mediated drug delivery enhances the cytotoxicity of Paclitaxel in autologous prostate cancer cells, J. Control. Release. 220 (2015) 727–737. doi:10.1016/j.jconrel.2015.09.031.

[38] M.S. JPK Armstrong, Strategic design of extracellular vesicle drug delivery systems, Adv. Drug Deliv. Rev. (2018) S0169–409X(18)30156–X.

[39] M. Garofalo, H. Saari, P. Somersalo, D. Crescenti, L. Kuryk, L. Aksela, C. Capasso, M. Madetoja, K. Koskinen, T. Oksanen, A. Mäkitie, M. Jalasvuori, V. Cerullo, P. Ciana, M. Yliperttula, Antitumor effect of oncolytic virus and paclitaxel encapsulated in extracellular vesicles for lung cancer treatment., J. Control. Release. 283 (2018) 223–234. doi:10.1016/j.jconrel.2018.05.015.

[40] P. Vader, X.O. Breakefield, M.J.A. Wood, Extracellular vesicles: Emerging targets for cancer therapy, Trends Mol. Med. 20 (2014) 385–393. doi:10.1016/j.molmed.2014.03.002.

[41] S.I. Ohno, G.P.C. Drummen, M. Kuroda, Focus on extracellular vesicles: Development of extracellular vesicle-based therapeutic systems, Int. J. Mol. Sci. 17 (2016). doi:10.3390/ijms17020172.

[42] K. Tang, Y. Zhang, H. Zhang, P. Xu, J. Liu, J. Ma, M. Lv, D. Li, F. Katirai, G.X. Shen, G.

ACCEPTED MANUSCRIPT

Zhang, Z.H. Feng, D. Ye, B. Huang, Delivery of chemotherapeutic drugs in tumour cell-derived microparticles, Nat. Commun. 3 (2012) 1211–1282. doi:10.1038/ncomms2282.

[43] R. van der Meel, M.H.A.M. Fens, P. Vader, W.W. van Solinge, O. Eniola-Adefeso, R.M. Schiffelers, Extracellular vesicles as drug delivery systems: Lessons from the liposome field, J. Control. Release. 195 (2014) 72–85. doi:10.1016/J.JCONREL.2014.07.049.

[44] M.A. Morse, J. Garst, T. Osada, S. Khan, A. Hobeika, T.M. Clay, N. Valente, R. Shreeniwas, M.A. Sutton, A. Delcayre, D.H. Hsu, J.B. Le Pecq, H.K. Lyerly, A phase I study of dexosome immunotherapy in patients with advanced non-small cell lung cancer, J. Transl. Med. 3 (2005) 1–8. doi:10.1186/1479-5876-3-9.

[45] S. Dai, D. Wei, Z. Wu, X. Zhou, X. Wei, H. Huang, G. Li, Phase I clinical trial of autologous ascites-derived exosomes combined with GM-CSF for colorectal cancer, Mol. Ther. 16 (2008) 782–790. doi:10.1038/mt.2008.1.

[46] S.C. Jang, O.Y. Kim, C.M. Yoon, D.S. Choi, T.Y. Roh, J. Park, J. Nilsson, J. Lötvall, Y.K. Kim, Y.S. Gho, Bioinspired exosome-mimetic nanovesicles for targeted delivery of chemotherapeutics to malignant tumors, ACS Nano. 7 (2013) 7698–7710. doi:10.1021/nn402232g.

[47] C. Grange, M. Tapparo, S. Bruno, D. Chatterjee, P.J. Quesenberry, C. Tetta, G. Camussi, Biodistribution of mesenchymal stem cell-derived extracellular vesicles in a model of acute kidney injury monitored by optical imaging, Int. J. Mol. Med. 33 (2014) 1055–1063. doi:10.3892/ijmm.2014.1663.

[48] T. Smyth, M. Kullberg, N. Malik, P. Smith-Jones, M.W. Graner, T.J. Anchordoquy, Biodistribution and delivery efficiency of unmodified tumor-derived exosomes, J. Control. Release. 199 (2015) 145–155. doi:10.1016/J.JCONREL.2014.12.013.

[49] P. Gangadaran, X.J. Li, H.W. Lee, J.M. Oh, S. Kalimuthu, R.L. Rajendran, S.H. Son, S.H. Baek, T.D. Singh, L. Zhu, S.Y. Jeong, S.-W. Lee, J. Lee, B.-C. Ahn, A new bioluminescent reporter system to study the biodistribution of systematically injected tumor-derived bioluminescent extracellular vesicles in mice, Oncotarget. 8 (2017) 109894–109914. doi:10.18632/oncotarget.22493.

[50] V. Cerullo, I. Diaconu, V. Romano, M. Hirvinen, M. Ugolini, S. Escutenaire, S.L. Holm, A. Kipar, A. Kanerva, A. Hemminki, An oncolytic adenovirus enhanced for toll-like receptor 9 stimulation increases antitumor immune responses and tumor clearance, Mol. Ther. 20 (2012) 2076–2086. doi:10.1038/mt.2012.137.

[51] R. Jannat, D. Hsu, G. Maheshwari, Inactivation of adenovirus type 5 by caustics, Biotechnol. Prog. 21 (2005) 446–450. doi:10.1021/bp049812f.

ACCEPTED MANUSCRIPT

[52] M. Garofalo, A. Villa, N. Rizzi, L. Kuryk, V. Mazzaferro, P. Ciana, Systemic Administration and Targeted Delivery of Immunogenic Oncolytic Adenovirus Encapsulated in Extracellular Vesicles for Cancer Therapies, Viruses. 10 (2018) 558. doi:10.3390/v10100558.

[53] R.F. Thompson, M. Walker, C.A. Siebert, S.P. Muench, N.A. Ranson, An introduction to sample preparation and imaging by cryo-electron microscopy for structural biology, Methods. 100 (2016) 3–15. doi:10.1016/j.ymeth.2016.02.017.

[54] N. Rizzi, M. Rebecchi, G. Levandis, P. Ciana, A. Maggi, Identification of novel loci for the generation of reporter mice, Nucleic Acids Res. 45 (2016) 1–14. doi:10.1093/nar/gkw1142.

[55] A. Koski, L. Kangasniemi, S. Escutenaire, S. Pesonen, V. Cerullo, I. Diaconu, P. Nokisalmi, M. Raki, M. Rajecki, K. Guse, T. Ranki, M. Oksanen, S.-L. Holm, E. Haavisto, A. Karioja-Kallio, L. Laasonen, K. Partanen, M. Ugolini, A. Helminen, E. Karli, P. Hannuksela, S. Pesonen, T. Joensuu, A. Kanerva, A. Hemminki, Treatment of cancer patients with a serotype 5/3 chimeric oncolytic adenovirus expressing GMCSF., Mol. Ther. 18 (2010) 1874–84. doi:10.1038/mt.2010.161.

[56] N. Woller, E. GÃ¼rlevik, C.-I. Ureche, A. Schumacher, F. KÃ¼hnel, Oncolytic Viruses as Anticancer Vaccines, Front. Oncol. 4 (2014) 1–13. doi:10.3389/fonc.2014.00188.

[57] C. Capasso, M. Hirvinen, M. Garofalo, D. Romaniuk, L. Kuryk, T. Sarvela, A. Vitale, M. Antopolsky, A. Magarkar, T. Viitala, T. Suutari, A. Bunker, M. Yliperttula, A. Urtti, V. Cerullo, Oncolytic adenoviruses coated with MHC-I tumor epitopes increase the antitumor immunity and efficacy against melanoma, Oncoimmunology. 5 (2016) 1–11. doi:10.1080/2162402X.2015.1105429.

[58] O. Kepp, L. Senovilla, I. Vitale, Consensus guidelines for the detection of immunogenic cell death, …. (2014) 1–19. doi:10.4161/21624011.2014.955691.

[59] B. György, T.G. Szabó, M. Pásztói, Z. Pál, P. Misják, B. Aradi, V. László, É. Pállinger, E. Pap, Á. Kittel, G. Nagy, A. Falus, E.I. Buzás, Membrane vesicles, current state-of-the-art: Emerging role of extracellular vesicles, Cell. Mol. Life Sci. 68 (2011) 2667–2688. doi:10.1007/s00018-011-0689-3.

[60] D.G. Meckes, N. Raab-Traub, Microvesicles and Viral Infection, J. Virol. 85 (2011) 12844–12854. doi:10.1128/JVI.05853-11.

[61] S.I. Ohno, M. Takanashi, K. Sudo, S. Ueda, A. Ishikawa, N. Matsuyama, K. Fujita, T. Mizutani, T. Ohgi, T. Ochiya, N. Gotoh, M. Kuroda, Systemically injected exosomes targeted to EGFR deliver antitumor microrna to breast cancer cells, Mol. Ther. 21 (2013) 185–191. doi:10.1038/mt.2012.180.

[62] G. Marelli, A. Howells, N.R. Lemoine, Y. Wang, Oncolytic viral therapy and the immune

ACCEPTED MANUSCRIPT

system: A double-edged sword against cancer, Front. Immunol. 9 (2018) 1–8. doi:10.3389/fimmu.2018.00866.

[63] L. Ran, X. Tan, Y. Li, H. Zhang, R. Ma, T. Ji, W. Dong, T. Tong, Y. Liu, D. Chen, X. Yin, X. Liang, K. Tang, J. Ma, Y. Zhang, X. Cao, Z. Hu, X. Qin, B. Huang, Delivery of oncolytic adenovirus into the nucleus of tumorigenic cells by tumor microparticles for virotherapy, Biomaterials. 89 (2016) 56–66. doi:10.1016/j.biomaterials.2016.02.025.

[64] C. Capasso, D. Cardella, M. Muller, M. Garofalo, L. Kuryk, K. Peltonen, V. Cerullo, 408. Oncolytic Vaccines in Combination with PD-L1 Blockade for the Treatment of Melanoma, Mol. Ther. 24 (2016) S161–S162. doi:10.1016/S1525-0016(16)33217-8.

[65] C.N. Chao, M.C. Lin, C.Y. Fang, P.L. Chen, D. Chang, C.H. Shen, M. Wang, Gene Therapy for Human Lung Adenocarcinoma Using a Suicide Gene Driven by a Lung-Specific Promoter Delivered by JC Virus-Like Particles, PLoS One. 11 (2016) e0157865. doi:10.1371/journal.pone.0157865.

[66] S.A.A. Kooijmans, P. Vader, S.M. van Dommelen, W.W. van Solinge, R.M. Schiffelers, Exosome mimetics: A novel class of drug delivery systems, Int. J. Nanomedicine. 7 (2012) 1525–1541. doi:10.2147/IJN.S29661.

[67] K.B. Johnsen, J.M. Gudbergsson, M.N. Skov, L. Pilgaard, T. Moos, M. Duroux, A comprehensive overview of exosomes as drug delivery vehicles - Endogenous nanocarriers for targeted cancer therapy, Biochim. Biophys. Acta - Rev. Cancer. 1846 (2014) 75–87. doi:10.1016/j.bbcan.2014.04.005.

[68] P. Vader, E.A. Mol, G. Pasterkamp, R.M. Schiffelers, Extracellular vesicles for drug delivery, Adv. Drug Deliv. Rev. 106 (2016) 148–156. doi:10.1016/j.addr.2016.02.006.

[69] N. Tominaga, Y. Yoshioka, T. Ochiya, A novel platform for cancer therapy using extracellular vesicles, Adv. Drug Deliv. Rev. 95 (2015) 50–55. doi:10.1016/j.addr.2015.10.002.

[70] X. Zhu, M. Badawi, S. Pomeroy, D.S. Sutaria, Z. Xie, A. Baek, J. Jiang, O.A. Elgamal, X. Mo, K. La Perle, J. Chalmers, T.D. Schmittgen, M.A. Phelps, Comprehensive toxicity and immunogenicity studies reveal minimal effects in mice following sustained dosing of extracellular vesicles derived from HEK293T cells, J. Extracell. Vesicles. 6 (2017). doi:10.1080/20013078.2017.1324730.

[71] T.M. Green, M.L. Alpaugh, S.H. Barsky, G. Rappa, A. Lorico, Breast cancer-derived extracellular vesicles: Characterization and contribution to the metastatic phenotype, Biomed Res. Int. 2015 (2015). doi:10.1155/2015/634865.

[72] K. Nakamura, K. Sawada, Y. Kinose, A. Yoshimura, A. Toda, E. Nakatsuka, K. Hashimoto, S. Mabuchi, K. Morishige, H. Kurachi, E. Lengyel, T. Kimura, Exosomes Promote Ovarian

ACCEPTED MANUSCRIPT

Cancer Cell Invasion through Transfer of CD44 to Peritoneal Mesothelial Cells, Mol. Cancer Res. 15 (2017) 78–92. doi:10.1158/1541-7786.MCR-16-0191.

[73] A. MacKenzie, H.L. Wilson, E. Kiss-Toth, S.K. Dower, R.A. North, A. Surprenant, Rapid secretion of interleukin-1β by microvesicle shedding, Immunity. 15 (2001) 825–835. doi:10.1016/S1074-7613(01)00229-1.

[74] C. Pizzirani, D. Ferrari, P. Chiozzi, E. Adinolfi, D. Sandona, E. Savaglio, F. Di Virgilio, Stimulation of P2 receptors causes release of IL-1beta-loaded microvesicles from human dendritic cells, Blood. 109 (2007) 3856–3864. doi:blood-2005-06-031377 [pii]\r10.1182/blood-2005-06-031377.

[75] E. Boilard, P.A. Nigrovic, K. Larabee, G.F.M. Watts, S. Jonathan, M.E. Weinblatt, E.M. Massarotti, E.R. Donnell, W. Farndale, J. Ware, D.M. Lee, NIH Public Access, 327 (2010) 580–583. doi:10.1126/science.1181928.Platelets.

[76] S. Gulinelli, E. Salaro, M. Vuerich, D. Bozzato, C. Pizzirani, G. Bolognesi, M. Idzko, F. Di Virgilio, D. Ferrari, IL-18 associates to microvesicles shed from human macrophages by a LPS/TLR-4 independent mechanism in response to P2X receptor stimulation, Eur. J. Immunol. 42 (2012) 3334–3345. doi:10.1002/eji.201142268.

[77] M. Baj-Krzyworzeka, K. Węglarczyk, B. Mytar, R. Szatanek, J. Baran, M. Zembala, Tumour-derived microvesicles contain interleukin-8 and modulate production of chemokines by human monocytes, Anticancer Res. 31 (2011) 1329–1335.

[78] O.P. Barry, D. Praticò, J.A. Lawson, G.A. FitzGerald, Transcellular activation of platelets and endothelial cells by bioactive lipids in platelet microparticles, J. Clin. Invest. 99 (1997) 2118–2127. doi:10.1172/JCI119385.

[79] J. Esser, U. Gehrmann, F.L. D'Alexandri, A.M. Hidalgo-Estévez, C.E. Wheelock, A. Scheynius, S. Gabrielsson, O. Rdmark, Exosomes from human macrophages and dendritic cells contain enzymes for leukotriene biosynthesis and promote granulocyte migration, J. Allergy Clin. Immunol. 126 (2010). doi:10.1016/j.jaci.2010.06.039.

[80] M. Shimoda, R. Khokha, Proteolytic factors in exosomes, Proteomics. 13 (2013) 1624–1636. doi:10.1002/pmic.201200458.

[81] K. Ohshima, K. Inoue, A. Fujiwara, K. Hatakeyama, K. Kanto, Y. Watanabe, K. Muramatsu, Y. Fukuda, S.I. Ogura, K. Yamaguchi, T. Mochizuki, Let-7 microRNA family Is selectively secreted into the extracellular environment via exosomes in a metastatic gastric cancer cell line, PLoS One. 5 (2010) 1–10. doi:10.1371/journal.pone.0013247.

[82] S.M. Lehmann, C. Krüger, B. Park, K. Derkow, K. Rosenberger, J. Baumgart, T. Trimbuch, G. Eom, M. Hinz, D. Kaul, P. Habbel, R. Kälin, E. Franzoni, A. Rybak, D. Nguyen, R. Veh, O.

ACCEPTED MANUSCRIPT

Ninnemann, O. Peters, R. Nitsch, F.L. Heppner, D. Golenbock, E. Schott, H.L. Ploegh, F.G. Wulczyn, S. Lehnardt, An unconventional role for miRNA: Let-7 activates Toll-like receptor 7 and causes neurodegeneration, Nat. Neurosci. 15 (2012) 827–835. doi:10.1038/nn.3113.

[83] S.I. Grivennikov, F.R. Greten, M. Karin, Immunity, Inflammation, and Cancer, Cell. 140 (2011) 883–899. doi:10.1016/j.cell.2010.01.025.Immunity.

[84] J.M. Pitt, A. Marabelle, A. Eggermont, J.C. Soria, G. Kroemer, L. Zitvogel, Targeting the tumor microenvironment: Removing obstruction to anticancer immune responses and immunotherapy, Ann. Oncol. 27 (2016) 1482–1492. doi:10.1093/annonc/mdw168.

[85] K.P. Krafts, The hidden drama Tissue repair, Organogenesis. 6 (2010) 225–233. doi:10.4161/org6.4.12555.

[86] Z. Julier, A.J. Park, P.S. Briquez, M.M. Martino, Promoting tissue regeneration by modulating the immune system, Acta Biomater. 53 (2017) 13–28. doi:10.1016/j.actbio.2017.01.056.

[87] L. Kuryk, A.-S.W. Møller, M. Garofalo, V. Cerullo, S. Pesonen, R. Alemany, M. Jaderberg, Anti-tumor specific T-cell responses induced by oncolytic adenovirus ONCOS-102 in peritoneal mesothelioma mouse model, J. Med. Virol. (2018) 1–5. doi:10.1002/jmv.25229.

[88] O.Y. Kim, J. Lee, Y.S. Gho, Extracellular vesicle mimetics: Novel alternatives to extracellular vesicle-based theranostics, drug delivery, and vaccines, Semin. Cell Dev. Biol. 67 (2017) 74–82. doi:10.1016/j.semcdb.2016.12.001.

[89] M. Yáñez-Mó, P.R.M. Siljander, Z. Andreu, A.B. Zavec, F.E. Borràs, E.I. Buzas, K. Buzas, E. Casal, F. Cappello, J. Carvalho, E. Colás, A. Cordeiro-Da Silva, S. Fais, J.M. Falcon-Perez, I.M. Ghobrial, B. Giebel, M. Gimona, M. Graner, I. Gursel, M. Gursel, N.H.H. Heegaard, A. Hendrix, P. Kierulf, K. Kokubun, M. Kosanovic, V. Kralj-Iglic, E.M. Krämer-Albers, S. Laitinen, C. Lässer, T. Lener, E. Ligeti, A. Line, G. Lipps, A. Llorente, J. Lötvall, M. Manček-Keber, A. Marcilla, M. Mittelbrunn, I. Nazarenko, E.N.M. Nolte-'t Hoen, T.A. Nyman, L. O'Driscoll, M. Olivan, C. Oliveira, É. Pállinger, H.A. Del Portillo, J. Reventós, M. Rigau, E. Rohde, M. Sammar, F. Sánchez-Madrid, N. Santarém, K. Schallmoser, M.S. Ostenfeld, W. Stoorvogel, R. Stukelj, S.G. Van Der Grein, M. Helena Vasconcelos, M.H.M. Wauben, O. De Wever, Biological properties of extracellular vesicles and their physiological functions, J. Extracell. Vesicles. 4 (2015) 1–60. doi:10.3402/jev.v4.27066.

[90] D. Ingato, J.U. Lee, S.J. Sim, Y.J. Kwon, Good things come in small packages: Overcoming challenges to harness extracellular vesicles for therapeutic delivery, J. Control. Release. 241 (2016) 174–185. doi:10.1016/j.jconrel.2016.09.016.

[91] S. Sharma, K. Das, J.R. Woo, J.K. Gimzewski, Nanofilaments on glioblastoma exosomes revealed by peak force microscopy, J. R. Soc. Interface. 11 (2014).

ACCEPTED MANUSCRIPT

doi:10.1098/rsif.2013.1150.

[92] A. Hoshino, B. Costa-Silva, T.L. Shen, G. Rodrigues, A. Hashimoto, M. Tesic Mark, H. Molina, S. Kohsaka, A. Di Giannatale, S. Ceder, S. Singh, C. Williams, N. Soplop, K. Uryu, L. Pharmer, T. King, L. Bojmar, A.E. Davies, Y. Ararso, T. Zhang, H. Zhang, J. Hernandez, J.M. Weiss, V.D. Dumont-Cole, K. Kramer, L.H. Wexler, A. Narendran, G.K. Schwartz, J.H. Healey, P. Sandstrom, K. Jørgen Labori, E.H. Kure, P.M. Grandgenett, M.A. Hollingsworth, M. De Sousa, S. Kaur, M. Jain, K. Mallya, S.K. Batra, W.R. Jarnagin, M.S. Brady, O. Fodstad, V. Muller, K. Pantel, A.J. Minn, M.J. Bissell, B.A. Garcia, Y. Kang, V.K. Rajasekhar, C.M. Ghajar, I. Matei, H. Peinado, J. Bromberg, D. Lyden, Tumour exosome integrins determine organotropic metastasis, Nature. 527 (2015) 329–335. doi:10.1038/nature15756.

ACCEPTED MANUSCRIPT

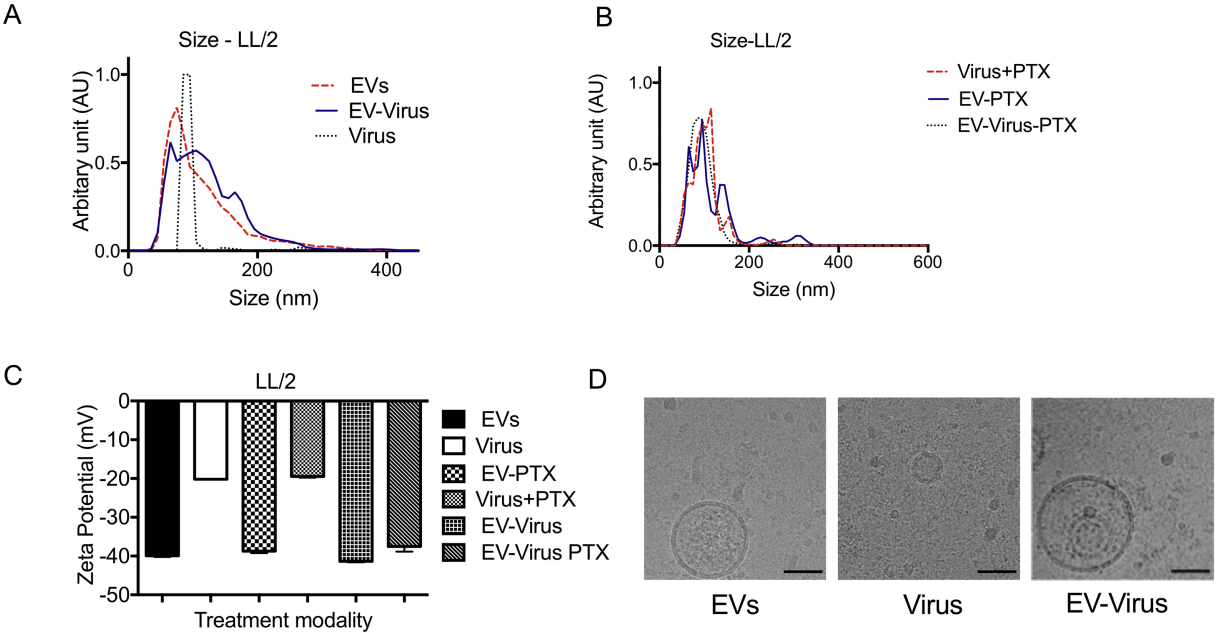
A
Size - LL/2
Arbitary unit (AU)
1.0
0.5
0.0
0
200
400
Size (nm)
EVs
EV-Virus
Virus
B
Size-LL/2
Arbitrary unit (AU)
1.0
0.5
0.0
0
200
400
600
Size (nm)
Virus+PTX
EV-PTX
EV-Virus-PTX
C
LL/2
Zeta Potential (mV)
0
-10
-20
-30
-40
-50
Treatment modality
EVs
Virus
EV-PTX
Virus+PTX
EV-Virus
EV-Virus PTX
D
EVs
Virus
EV-Virus

Figure 1

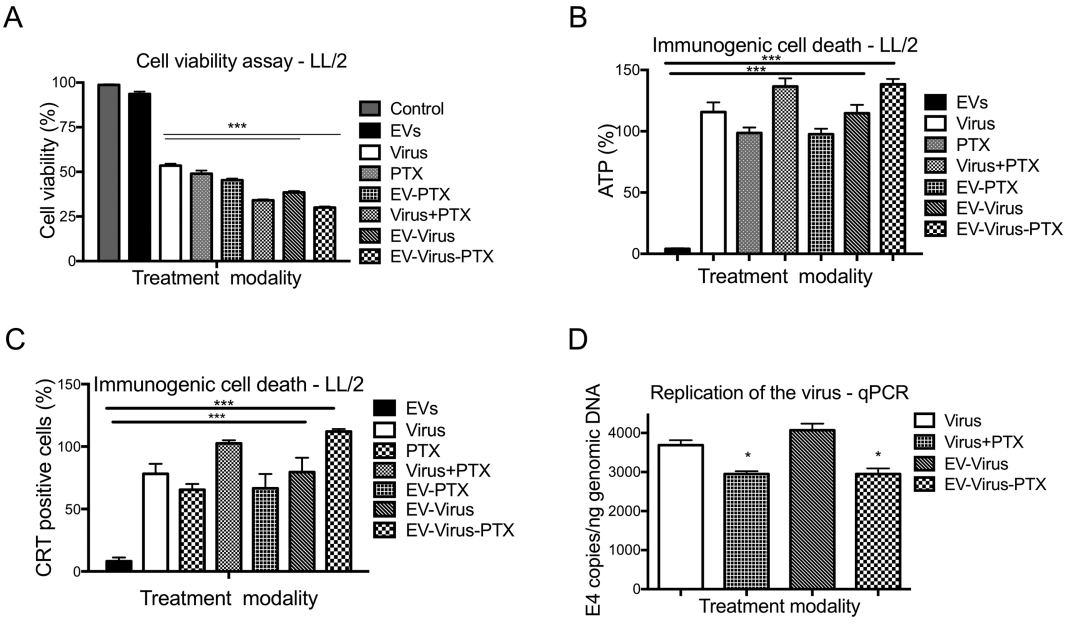
A
Cell viability assay - LL/2
Cell viability (%)
100
75
50
25
0
***
Control
EVs
Virus
PTX
EV-PTX
Virus+PTX
EV-Virus
EV-Virus-PTX
Treatment modality
B
Immunogenic cell death - LL/2
ATP (%)
150
100
50
0
***
***
EVs
Virus
PTX
Virus+PTX
EV-PTX
EV-Virus
EV-Virus-PTX
Treatment modality
C
Immunogenic cell death - LL/2
CRT positive cells (%)
150
100
50
0
***
***
EVs
Virus
PTX
Virus+PTX
EV-PTX
EV-Virus
EV-Virus-PTX
Treatment modality
D
Replication of the virus - qPCR
E4 copies/ng genomic DNA
4000
3000
2000
1000
0
*
*
Virus
Virus+PTX
EV-Virus
EV-Virus-PTX
Treatment modality

Figure 2

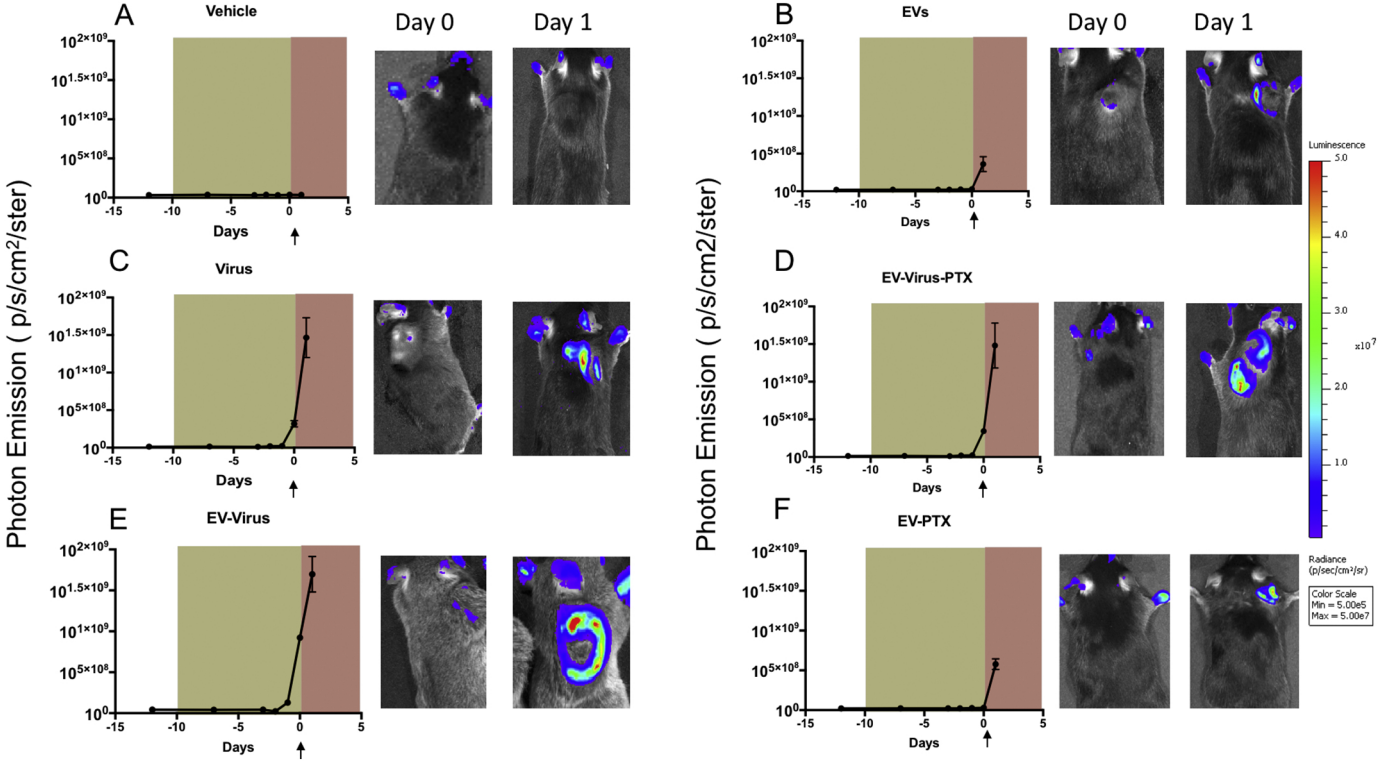
A
Vehicle
Day 0
Day 1
B
EVs
C
Virus
D
EV-Virus-PTX
E
EV-Virus
F
EV-PTX
Photon Emission (p/s/cm2/ster)
Days
Luminescence
x10^7
Radiance (p/sec/cm²/sr)
Color Scale
Min = 5.00e5
Max = 5.00e7

Figure 3

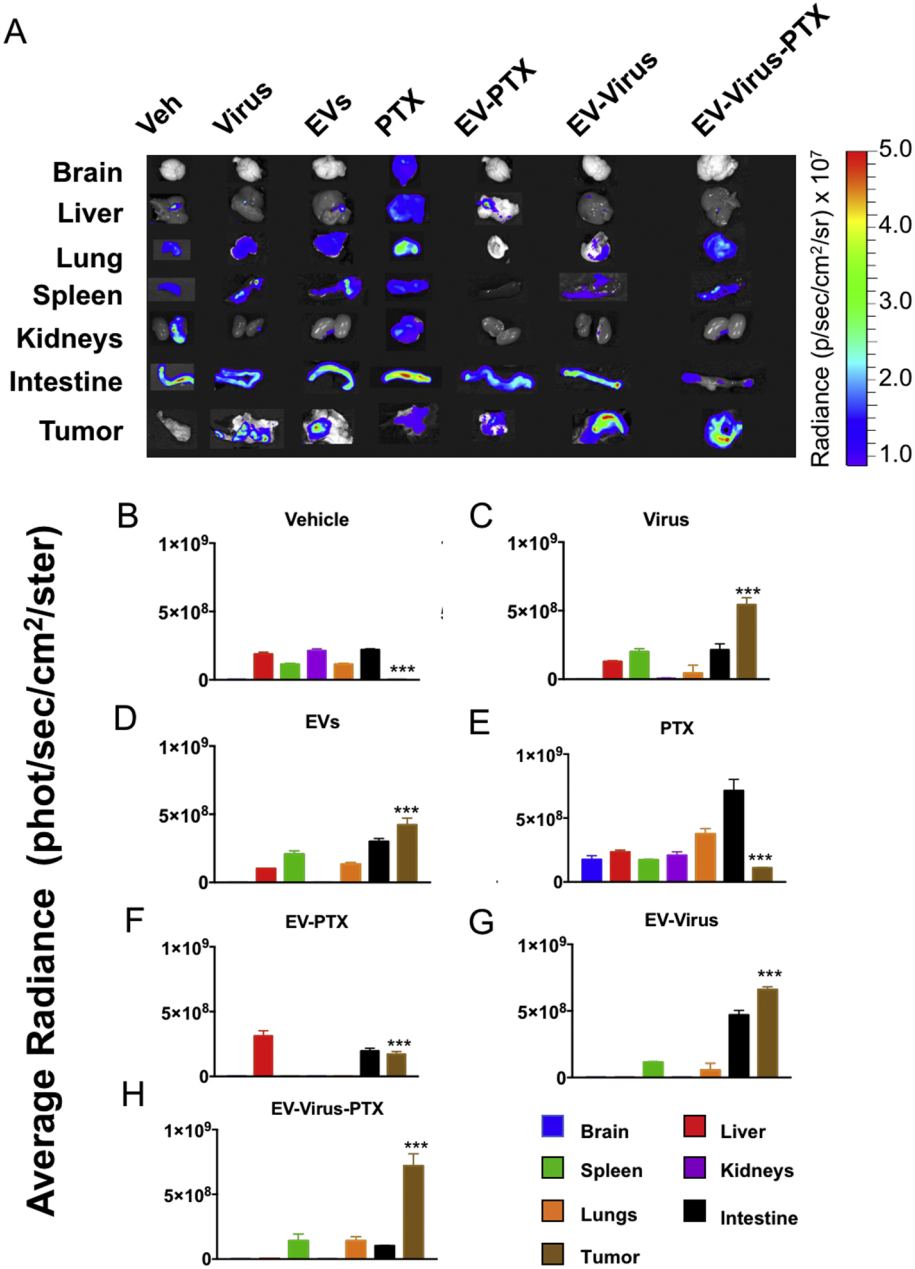
A
Veh
Virus
EVs
PTX
EV-PTX
EV-Virus
EV-Virus-PTX
Brain
Liver
Lung
Spleen
Kidneys
Intestine
Tumor
Radiance (p/sec/cm²/sr) x 10⁷
5.0
4.0
3.0
2.0
1.0
Average Radiance (phot/sec/cm²/ster)
B
Vehicle
C
Virus
D
EVs
E
PTX
F
EV-PTX
G
EV-Virus
H
EV-Virus-PTX
1×10⁹
5×10⁸
0
***
Brain
Liver
Spleen
Kidneys
Lungs
Intestine
Tumor

Figure 4

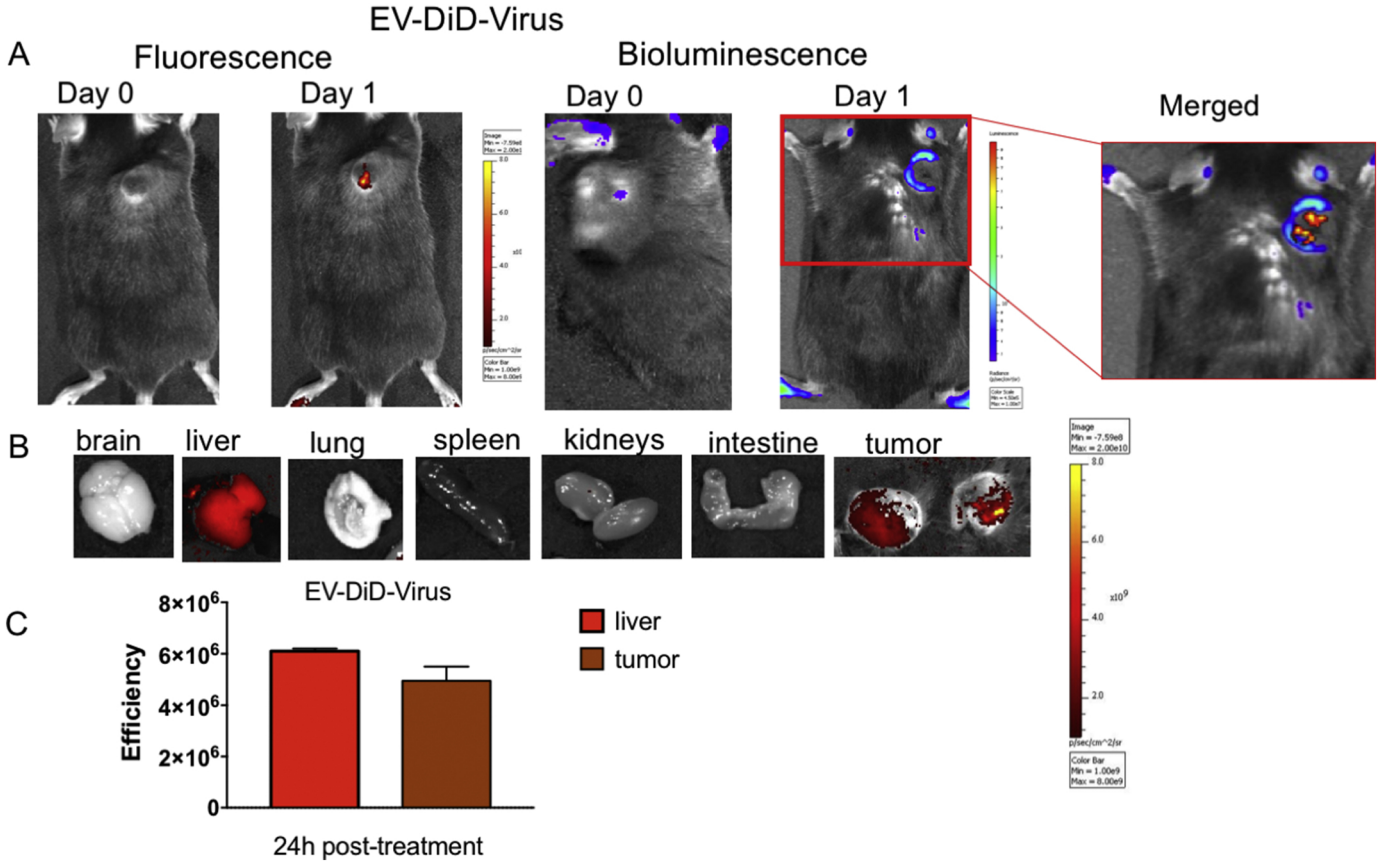
EV-DiD-Virus
A
Fluorescence
Bioluminescence
Day 0
Day 1
Day 0
Day 1
Merged
B
brain
liver
lung
spleen
kidneys
intestine
tumor
C
EV-DiD-Virus
liver
tumor
Efficiency
8×10^6
6×10^6
4×10^6
2×10^6
0
24h post-treatment

Figure 5

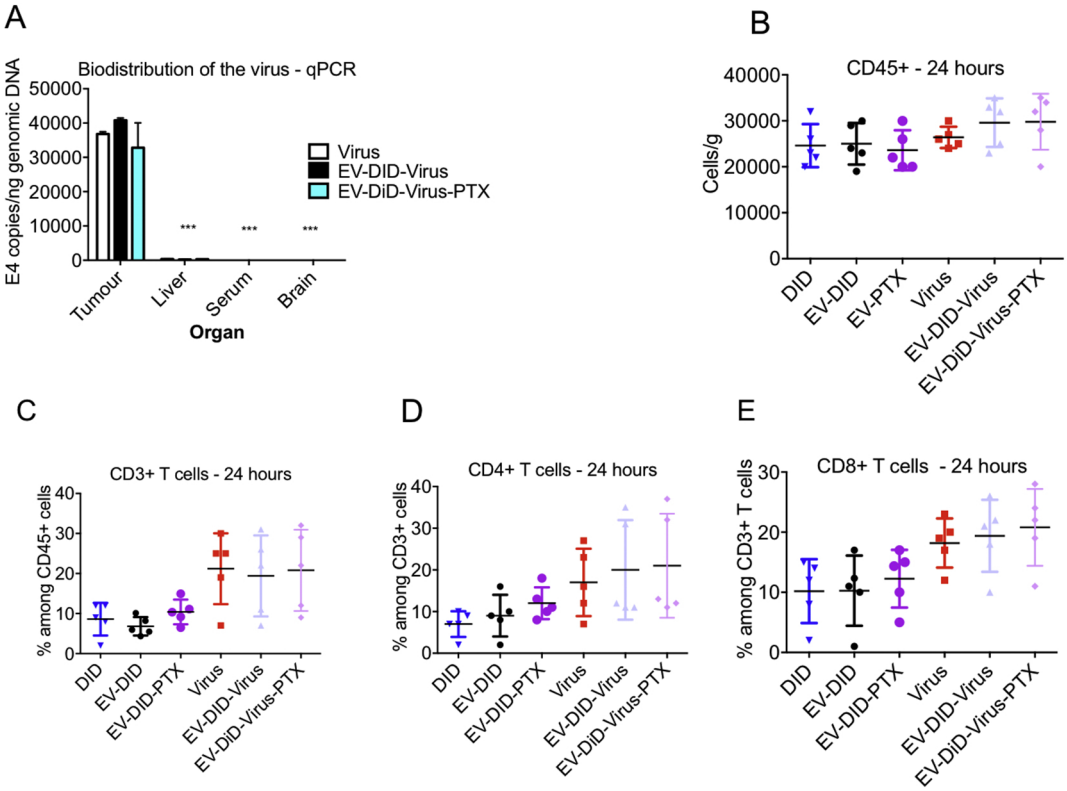
A
Biodistribution of the virus - qPCR
E4 copies/ng genomic DNA
50000
40000
30000
20000
10000
0
Virus
EV-DID-Virus
EV-DiD-Virus-PTX
***
***
***
Tumour
Liver
Serum
Brain
Organ
B
CD45+ - 24 hours
Cells/g
40000
30000
20000
10000
0
DID
EV-DID
EV-PTX
Virus
EV-DID-Virus
EV-DiD-Virus-PTX
C
CD3+ T cells - 24 hours
% among CD45+ cells
40
30
20
10
0
DID
EV-DID
EV-DID-PTX
Virus
EV-DID-Virus
EV-DiD-Virus-PTX
D
CD4+ T cells - 24 hours
% among CD3+ cells
40
30
20
10
0
DID
EV-DID
EV-DID-PTX
Virus
EV-DID-Virus
EV-DiD-Virus-PTX
E
CD8+ T cells - 24 hours
% among CD3+ T cells
30
20
10
0
DID
EV-DID
EV-DID-PTX
Virus
EV-DID-Virus
EV-DiD-Virus-PTX

Figure 6